heritage

Article

RADAR: A Framework for Risk Assessment and Degradation Analysis for Cultural Heritage Buildings Through CFD Modeling

Asimina Dimara [1,*], Mariya Pantusheva [2], Nikolaos-Alexios Stefanis [3], Orfeas Eleftheriou [4], Radostin Mitkov [2], Vasilis Naserentin [4,5], Dessislava Petrova-Antonova [2], Anders Logg [4] and Christos-Nikolaos Anagnostopoulos [1,*]

1 Department of Cultural Technology & Communication, University of the Aegean, 81100 Mytilene, Greece
2 Big Data for Smart Society Institute (GATE), Sofia University, 1504 Sofia, Bulgaria; mariya.pantusheva@gate-ai.eu (M.P.); radostin.mitkov@gate-ai.eu (R.M.); dessislava.petrova@gate-ai.eu (D.P.-A.)
3 Department of Conservation of Antiquities and Works of Art, University of West Attica, 11521 Athens, Greece; astefanis@uniwa.gr
4 Department of Mathematical Sciences, Chalmers University of Technology, SE-412 96 Gothenburg, Sweden; vasilis.naserentin@chalmers.se (V.N.); logg@chalmers.se (A.L.)
5 Department of Electrical & Computer Engineering, Aristotle University of Thessaloniki, 54124 Thessaloniki, Greece
* Correspondence: dimara@aegean.gr (A.D.); canag@aegean.gr (C.-N.A.)

Abstract

Cultural heritage buildings constitute an irreplaceable record of historical, social, and architectural identity, and their preservation is essential for cultural continuity and sustainable development. However, their conservation is inherently challenging due to material aging, complex construction techniques, limited documentation, and strict intervention constraints that restrict invasive monitoring or retrofitting solutions. Environmental degradation and microclimatic effects further accelerate deterioration, often in ways that are difficult to quantify or predict. This paper presents RADAR, a non-invasive, data-driven framework for assessing environmental and structural risk in cultural heritage buildings. The proposed approach integrates high-resolution geometric acquisition, computational fluid dynamics (CFD) modeling, and environmental monitoring to analyze airflow patterns, temperature distribution, and moisture-related decay mechanisms. By combining measured data with numerical simulations, RADAR enables the identification of high-risk zones and deterioration drivers without altering the building fabric. The framework is demonstrated through a real-world case study, illustrating its applicability as a decision-support tool for preventive conservation and heritage management.

Keywords: cultural heritage preservation; computational fluid dynamics (CFD); risk assessment; 3D visualization; digital twins; environmental degradation

Check for updates

Academic Editor: Athos Agapiou

Received: 3 February 2026
Revised: 27 February 2026
Accepted: 11 March 2026
Published: 12 March 2026

Copyright: © 2026 by the authors. Licensee MDPI, Basel, Switzerland. This article is an open access article distributed under the terms and conditions of the Creative Commons Attribution (CC BY) license.

1. Introduction

Cultural Heritage Buildings and Structures (CHBS) are significant because they serve as symbols of a community's or country's history, culture, and identity [1]. They are meaningful monuments that offer a concrete connection to the past while assisting people in understanding their origins and appreciating the accomplishments of their predecessors. It is of utmost importance to maintain cultural heritage structures to contribute to a city's or

region's continued diversity in terms of style and architecture [2]. Furthermore, the originality of each structure and its individual style and design add to the charm and beauty of the built environment. Moreover, cultural heritage structures offer an opportunity to learn about traditional building practices and craftsmanship by serving as a reminder of the abilities and methods of former generations [3]. Future construction projects can then use this information as a basis, preserving these talents for the benefit of the next generations.

CHBS are not only physical structures but carriers of tangible and intangible values, including historical, social, aesthetic, and identity-related dimensions [4]. International conservation doctrine has consistently emphasized the need to preserve authenticity, integrity, and cultural significance as central principles of heritage management [5]. Foundational documents such as the Venice Charter (ICOMOS, 1964), the Burra Charter (Australia ICOMOS, 2013), and UNESCO's World Heritage Convention highlight that heritage assets embody collective memory and social continuity, and therefore require careful, evidence-based conservation approaches [6]. Within this theoretical context, preventive conservation and risk-informed management are increasingly recognized as essential strategies for safeguarding heritage values while minimizing invasive interventions [7].

Buildings that are considered to be of cultural significance require regular maintenance. These structures, some of which are centuries old, are prone to deterioration over time as a result of multiple interacting factors, including aging, weathering, human activity, and structural stresses. In seismically active regions, such as the Mediterranean basin, seismic loading constitutes a critical source of structural vulnerability, potentially leading to cracking, material detachment, and progressive weakening of masonry systems [8]. One of the main reasons cultural heritage structures degrade is weathering [9]. Specifically, environmental factors such as temperature changes, wind, rain, and snow can all physically harm a building's materials and structure, resulting in erosion, corrosion, and fissures. Degradation is also influenced by aging because materials such as wood, stone, and brick deteriorate over time. Furthermore, cultural heritage structures can suffer deterioration as a result of human activity.

To stop additional harm and assure the long-term preservation of cultural heritage structures, regular maintenance is required [10]. Cleaning, fixing damage and cracks, changing out worn or damaged materials, and putting precautions in place to stop further deterioration are some examples of maintenance duties. Cultural heritage structures may sustain irreparable harm if upkeep is not provided, which could result in their eventual loss. The loss of these structures could be significant from both an aesthetic and a cultural and historical standpoint because they are frequently a vital component of a nation's cultural legacy and identity. Consequently, it is crucial to give regular maintenance of these buildings top priority.

Nonetheless, to preserve the historical and cultural importance of these buildings, restrictions on interference are frequently put in place. These limitations may be in the form of planning laws, legal regulations, or construction codes, among others [11]. The necessity for the preservation or conservation of the original building materials, architecture, and layout is one typical sort of restriction [12]. This means that any improvements must be made to the building while maintaining its historic significance and architectural value. In most regulatory contexts, interventions in CHBs are subject to formal authorization procedures led by competent state authorities, such as Ministries of Culture or designated heritage agencies responsible for the classification and protection of listed buildings. Any significant alterations or conservation measures typically require prior approval from these authorities to ensure compliance with preservation legislation. Community organizations, local government bodies, and heritage specialists often participate in a consultative or supporting role, contributing expertise and facilitating broader social acceptance of proposed

interventions. This makes it easier to guarantee that the modifications are in keeping with the building's cultural and historical significance and that the larger community will accept and support them.

Respectively, non-intrusive risk analysis and degradation techniques for CHBS are of great consequence as they may indicate possible risks while being a basic input for predictive or even prescriptive maintenance. Non-intrusive risk analysis for CHBS deterioration is an area of active research in the field of heritage conservation [13]. While there is some literature on the topic, there are still significant gaps in our understanding of how to carry out non-intrusive risk analysis effectively. To begin with, there is a need for the creation of non-intrusive monitoring methods that can deliver precise and trustworthy information on the state of cultural heritage structures [14]. Frameworks for assessing risk must be created that take into consideration the special features of structures with cultural heritage [14]. Respectively, this necessitates knowledge of the elements that influence building deterioration, such as the surroundings, structural layout, and material characteristics. This necessitates the creation of non-intrusive technique procedures and guidelines, as well as instruction for conservation specialists on how to use these techniques successfully.

International conservation doctrine further frames the conditions under which interventions in historic buildings may occur. Principles such as minimum intervention, reversibility of conservation measures, and clear differentiation between original and new materials are consistently emphasized in documents issued by UNESCO and ICOMOS [15]. These guidelines aim to preserve authenticity and material integrity while allowing necessary conservation actions. Within this regulatory and ethical framework, non-intrusive assessment techniques gain particular importance, as they support informed decision-making without compromising the historic fabric.

Within this context, the current paper suggests a novel framework for the Risk Assessment and Degradation Analysis Report (RADAR) for CHBS based on Computational Fluid Dynamics (CFD) modeling. The RADAR framework was developed through the integration of established principles in preventive conservation, environmental exposure assessment, and physics-based numerical modeling. It builds upon prior research in environmental monitoring and CFD-based heritage analysis, consolidating these elements into a structured workflow for exposure-driven risk assessment. In the present formulation, CFD modeling is an intrinsic and indispensable component of RADAR, providing the quantitative basis for spatially resolved environmental risk indicators. The framework is therefore explicitly designed around physics-based simulation as a core analytical mechanism rather than as an optional extension. The main novelties addressed are:

- Non-intrusive data acquisition, analysis, reporting of the CHBS leveraging open data sets and weather stations.
- Procedures for non-intrusive techniques including a framework for conservation specialists on how to use these techniques effectively.
- A robust framework for visualizing and assessing potential risk hazards for CHBS.
- A general workflow for CFD analysis of cultural heritage sites subjected to environmental exposures. This workflow provides insights into the modeling process on a step-by-step basis, starting with the required input data, its pre-processing, solution setup and post-processing of the results for their seamless integration into the RADAR framework.
- Exploring and testing the effectiveness of different preservation measures in a virtual environment (through simulations) before applying them to the real site, thus minimizing preservation costs and even avoiding further deterioration of the structure caused by potentially unsuitable measures.

The rest of the paper is structured as follows. The Research Aim Section presents the motivation and context of this work, outlining the conservation challenges addressed and the rationale for the proposed approach. Section 2 reviews related work on digital documentation, environmental monitoring, and simulation-based risk assessment for cultural heritage buildings. Section 3 describes the proposed methodology, including the RADAR framework, data acquisition pipeline, and the numerical and analytical procedures adopted. Section 4 presents the case study (the castle of Mytilene), reporting the experimental setup and the main results derived from measurements and simulations. Finally, Section 6 concludes the paper and discusses limitations and directions for future work.

Research Aim

Environmental exposure, particularly wind and wind-driven rain, represents one of the most critical drivers of material deterioration in CHBS [16,17]. Wind contributes not only through mechanical loading but also through the transport of moisture, salts, airborne particles, and biological agents, accelerating erosion, infiltration, and surface degradation. The conceptual interactions between climatic and non-climatic wind effects are illustrated in Figure 1.

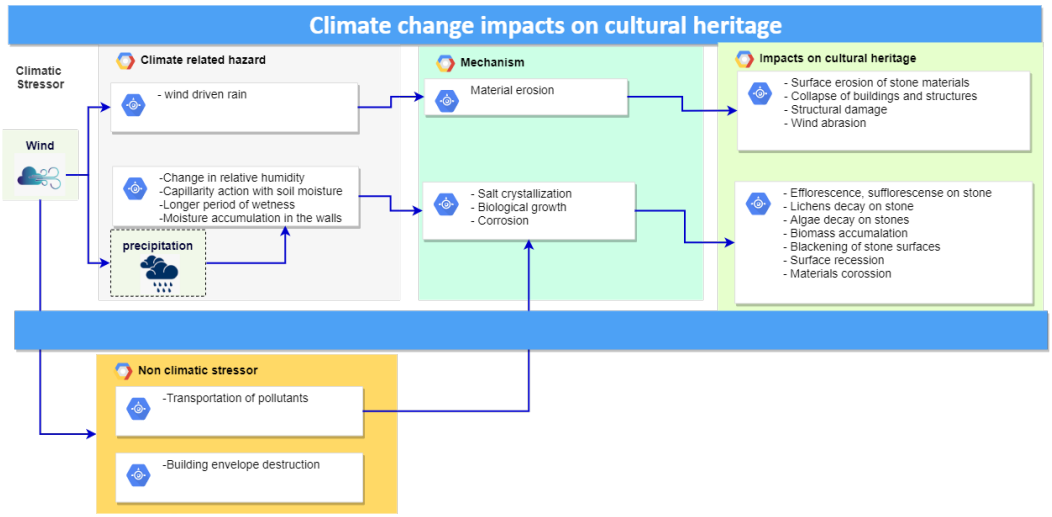


Figure 1. Climate and non-climate wind impacts on cultural heritage. Conceptual diagram developed by the authors, based on Sesana et al. (2021) [17].

Despite increasing awareness of these processes, practical tools capable of systematically quantifying wind-related exposure under non-intrusive and regulatory-constrained conditions remain limited. In many heritage contexts, invasive monitoring or extensive on-site instrumentation is either restricted or not feasible. The primary aim of this study is therefore to develop and validate a non-invasive, data-driven framework for exposure-based risk assessment of CHBS. By integrating geometric modeling, open environmental datasets, and CFD simulation, the proposed RADAR framework enables spatial identification of vulnerability zones and supports preventive conservation decision-making without physical intervention.

2. State of the Art

This section reviews state-of-the-art methods for non-invasive assessment of cultural heritage buildings, focusing on digital surveying, environmental monitoring, and physics-based numerical simulation approaches, with particular emphasis on CFD applications. Limitations of existing methodologies are discussed to position the contribution of the proposed framework.

2.1. Degradation and Risk Assessment Techniques

In the field of building degradation and risk assessment (RA), an extensive body of research has contributed to the development of comprehensive methodologies. Visual inspections, often considered the foundation of building assessment, have been extensively explored [18,19]. Additionally, non-destructive testing (NDT) methods have gained prominence, with [19] highlighting their efficacy in identifying hidden structural defects. The integration of sensor networks and Internet of Things (IoT) technologies has been examined in-depth by [20], providing real-time data for continuous monitoring. Furthermore, the utilization of artificial intelligence (AI) and machine learning (ML) techniques in building assessment has seen notable advancements, as demonstrated by the work of [21,22]. These combined efforts have shaped the multifaceted landscape of building degradation and risk assessment, offering a holistic approach to ensuring structural integrity and safety.

Furthermore, CHBS pose a distinct set of challenges, necessitating specialized strategies for degradation and risk assessment to safeguard their historical and architectural significance. The use of 3D laser scanning and digital modeling techniques has been extensively explored, enabling the creation of precise and detailed representations of CHBS [23]. In addition to structural considerations, cultural significance factors have been increasingly integrated into risk assessment models by [24], reflecting the importance of preserving the heritage value of these buildings. The work of [17] describes the role of climate change in CHBS degradation, underlining the need to address environmental factors. Furthermore, collaborative efforts by Zeng et al. [25] have emphasized the role of interdisciplinary teams, encompassing architects, engineers, and conservators, to develop holistic strategies for CHBS preservation. These diverse studies collectively contribute to a comprehensive approach to safeguarding the structural and cultural heritage of CHBS.

Table 1 highlights representative methodological directions in degradation and risk assessment research. The categorization reflects dominant technological and conceptual approaches rather than an exhaustive bibliographic survey. Overall, cultural heritage is crucial for identity but its value and vulnerability are often overlooked in risk assessments. These assessments are essential for identifying effective mechanisms for climate change adaptation and disaster management (Table 1). However, there is a lack of research on intangible aspects of heritage and their influence on risk and resilience. Most methods focus on exposure without considering vulnerability or adaptive capacity. Future assessments should include participatory approaches and community-scale values to better understand cultural heritage's role in adaptive capacity, vulnerability, and resilience [26].

Table 1. Summary of degradation and RA techniques.

Study	Aspect	Key Research Contributions
Conventional Buildings		
[18,19]	Visual Inspections	Extensively explored as a foundation of building assessment.
[19,27]	Non-Destructive Testing (NDT)	Highlighted for identifying hidden structural defects.
[20,28]	IoT and Sensor Networks	Examined for real-time data and continuous monitoring.
[21,22]	Artificial Intelligence and Machine Learning	Advancements in using AI/ML techniques for assessment.

Table 1. *Cont.*

Study	Aspect	Key Research Contributions
Cultural Heritage Buildings (CHBS)		
[23,29]	3D Laser Scanning and Digital Modeling	Used to create precise representations of CHBS.
[24,30]	Cultural Significance	Integration into risk assessment models for heritage preservation.
[17,31]	Climate Change	Considered for its impact on CHBS degradation.
[25,32]	Interdisciplinary Collaboration	Emphasized for holistic strategies involving various experts.

2.2. CFD in Cultural Heritage Preservation

CFD methods are employed to simulate and analyze airflow behavior around cultural sites as understanding airflow patterns and their effects on heritage buildings is essential for ensuring their long-term preservation. An early example of CFD's application to cultural heritage is the investigation of the wind environment over the expansive area of the Giza Pyramids, encompassing the Great Sphinx monument [33]. It focuses on estimating wind pressure and surface friction distribution, which contributed to the erosion of the monuments' external surfaces by sand particles. Another example application of CFD in heritage conservation is related to the Crypt of the Cathedral of Lecce in Italy [34]. A digital model of the site was developed and CFD simulations were applied to study thermo-hygrometric parameters and airflow patterns. These simulations helped reproduce the crystallization of salts and the deterioration of artworks, facilitating the proposal of management scenarios to mitigate risky micro-climatic conditions.

Further research in [35] focused on the effect of wind erosion in the Yongling Mausoleum, China. By constructing a 3D model of the heritage site and employing CFD, the authors predicted erosion caused by wind on each monument within the Mausoleum complex and explored the role of vegetation in protecting the heritage buildings. Similarly, another study involved creating a 3D mesh for the heritage site in Baelo Claudia, Spain [36]. The application of CFD in this context allowed for the analysis of sand-loaded airflow erosion, and by incorporating environmental information, the deterioration of the site over the course of the next 50 and 100 years was predicted. In a more recent study, researchers focused on Kim Myeong-Kwan Gotaek, a wooden building of great cultural significance in Korea [37]. This study addressed the challenges posed by moisture and temperature, which are known to be problematic for architecture, necessitating an in-depth investigation to preserve this important cultural heritage site. Finally, another significant study explored the local climate of the cultural heritage site of Majianglong villages in China [9]. It sought to understand the influence of the village layout on the wind and thermal environment surrounding the heritage site by utilizing CFD simulations. These studies collectively exemplify the broad scope of CFD applications in cultural heritage preservation, encompassing various regions, architectural styles, and environmental challenges.

Although the amount of research on environmental degradation of cultural heritage has been increasing in recent years, many studies have focused on a single mechanism of degradation or have developed modeling techniques in isolation from one another. CFD-based modeling has increased in application; however, it is primarily used as a "case-by-case" tool for individual buildings, rather than an integral part of a structured and transferable risk assessment methodology. There is also little emphasis placed on quantifying uncertainty, validating the results of simulations, and translating simulation

data into useful conservation recommendations. As such, this paper presents RADAR, a non-destructive, data and physics-based framework that combines CFD modeling with a larger risk assessment and degradation analysis process for assessing the potential risks associated with environmental loading to cultural heritage buildings. This integrated framework allows the incorporation of environmental loads, exposure metrics and multiple scenarios in a systematic way to bridge the gap between the high fidelity simulations and the decisions made by specialists in relation to preventive conservation and maintenance of CHBS.

3. Methodology

This section describes the methodology adopted in this study and details the proposed RADAR framework. The workflow integrates data acquisition, geometric reconstruction, environmental monitoring, and numerical simulation to enable a non-invasive assessment of environmental and structural risk in cultural heritage buildings.

3.1. Overall RADAR Framework and Architecture

The RADAR methodology is structured as a layered and logically interconnected workflow that integrates heritage documentation, environmental exposure analysis, physics-based simulation, and risk-informed interpretation into a unified assessment framework. As illustrated in Figure 2, the architecture begins with heritage asset characterization, where documentation, material identification, and regulatory constraints define the baseline condition of the cultural heritage building. This stage establishes the contextual and physical parameters necessary for subsequent analysis. The second stage focuses on environmental exposure assessment, incorporating climatic data, wind characteristics, humidity trends, and pollutant indicators to identify dominant external stressors affecting the structure.

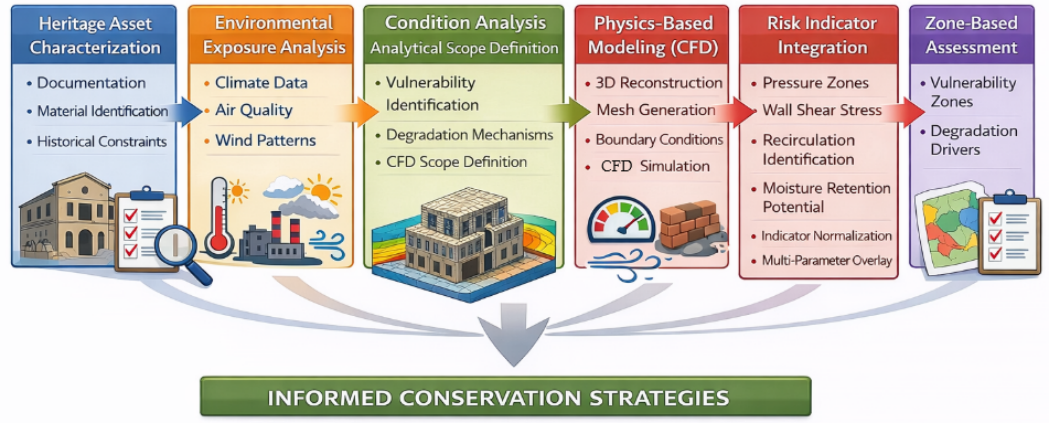


Figure 2. Overall RADAR framework architecture illustrating the sequential stages of heritage characterization, environmental exposure analysis, physics-based modeling, risk indicator integration, and zone-based assessment.

The third stage consists of condition analysis and analytical scope definition, which synthesizes heritage documentation and environmental exposure findings to identify vulnerable elements and dominant degradation mechanisms. This stage defines the objectives, parameters, and boundary conditions required for the subsequent computational analysis. The fourth stage introduces physics-based modeling through three-dimensional reconstruction and CFD simulation, enabling quantification of aerodynamic behavior and surface interaction mechanisms. The resulting parameters, such as pressure distribution, wall shear stress, and flow recirculation patterns, are processed within a dedicated risk indicator integration layer, where multiple exposure metrics are normalized and com-

bined. Subsequently, the framework translates these integrated indicators into spatially differentiated vulnerability zones and condition categories through a zone-based assessment stage. The final outcome supports informed and minimally invasive conservation strategies. This structured architecture ensures methodological transparency, interdisciplinary interpretability, and scalability of the RADAR framework across different cultural heritage contexts.

3.2. Heritage Asset Characterization

This stage establishes the baseline understanding of the heritage asset, including its historical context, architectural configuration, material system, and intervention constraints. The aim is to document the building with minimal intrusion and compile the information required for later exposure analysis and simulation. It includes (i) documentation and inventory, (ii) condition analysis supported by expert input and available records.

3.2.1. Documentation

Access to CHBS is frequently restricted due to their protected status, limiting opportunities for direct inspection and on-site documentation. In such cases, documentation must rely on non-intrusive sources such as archival material, publicly available imagery, geospatial platforms, and prior technical reports, complemented by expert interpretation. The objective of this stage is to establish a reliable baseline record of the asset, including its architectural configuration, material system, historical evolution, and known interventions. This structured inventory provides the foundational input for subsequent condition analysis and risk evaluation.

The documentation and inventory process includes the following steps (Figure 3):

i **Archival research:** Collection of historical documents, architectural drawings, photographs, and records of past modifications or repairs.
ii **Historical research and Geospatial data:** Integration of archival data with geospatial sources, such as satellite imagery and mapping platforms, to define orientation, urban context, and surrounding morphology.
iii **Engage Expert:** Collaboration with architects, historians, and conservation specialists to interpret documentation and produce coherent architectural descriptions.
iv **Remote Material Analysis:** Extraction of information regarding construction materials and previously identified vulnerabilities based on available documentation.
v **Collate Data Comprehensive Inventory** Compilation of all collected data into a structured inventory that supports condition analysis and subsequent modeling stages.

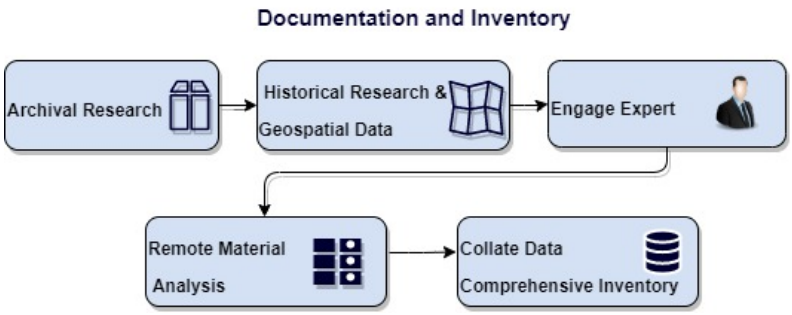


Figure 3. Documentation and inventory step-wise process.

3.2.2. Material Identification

Material identification aims to determine the composition, construction typology, and decay susceptibility of the building fabric. For CHBS, direct sampling or destructive testing is often restricted; therefore, material characterization is primarily based on archival

documentation, previous technical reports, photographic evidence, and expert interpretation. The process includes the identification of primary structural materials (e.g., masonry units, mortar types, timber, metal elements), surface finishes, and known repair layers. Particular attention is given to material-specific vulnerabilities, such as moisture absorption capacity, salt crystallization potential, freeze–thaw sensitivity, corrosion susceptibility, and abrasion resistance. These properties are essential for linking environmental exposure to plausible deterioration mechanisms.

When available, previous conservation reports and documented interventions are reviewed to assess compatibility issues between original and replacement materials. This stage establishes the material baseline required for interpreting environmental loads and CFD-derived indicators in terms of realistic degradation risks.

3.2.3. Historical and Regulatory Constraints

CHBS are subject to regulatory frameworks that govern intervention, documentation, and modification procedures. These constraints are typically defined by national heritage legislation and implemented through competent authorities such as Ministries of Culture or designated heritage agencies. Conservation doctrine emphasizes principles such as minimum intervention, reversibility, compatibility of materials, and preservation of authenticity. As a result, invasive testing, structural alterations, and extensive material sampling are often limited or require formal approval. These restrictions directly influence methodological choices, particularly regarding data acquisition and diagnostic techniques.

Within this context, the RADAR framework is intentionally designed as a non-intrusive assessment methodology. The reliance on existing documentation, environmental datasets, and physics-based simulation aligns with conservation principles while enabling evidence-based evaluation of environmental risk without compromising the historic fabric of the asset.

3.3. Environmental Exposure Analysis

Environmental exposure analysis quantifies the external stressors acting on a Cultural Heritage Building and defines the boundary conditions for subsequent physics-based modeling. This stage integrates climatic records, air quality indicators, and wind statistics to characterize both long-term degradation drivers and dominant aerodynamic loading conditions.

Climatic data are obtained from validated meteorological sources and include temperature variability, relative humidity trends, precipitation intensity, and seasonal patterns [38]. These parameters are analyzed to identify exposure conditions associated with moisture accumulation, freeze–thaw cycles, thermal stress, and material fatigue. Statistical descriptors such as annual averages and extreme events are extracted to establish representative environmental scenarios.

Air quality indicators are examined to assess pollutant-driven deterioration mechanisms. Parameters such as particulate matter (PM_{10}, $PM_{2.5}$), sulfur dioxide, nitrogen oxides, and, where relevant, marine salt aerosols are evaluated to estimate cumulative exposure. These factors are linked to processes such as surface erosion, black crust formation, corrosion, and chemical decay.

Wind patterns are analyzed using directional frequency distributions and wind rose data to identify prevailing directions, seasonal variability, and extreme gust conditions. Particular attention is given to wind-driven rain and localized acceleration effects induced by surrounding urban morphology. The results of this stage provide the aerodynamic input parameters and scenario definitions for the CFD simulations presented in the subsequent section.

3.4. Condition Analysis and Analytical Scope Definition

Condition analysis synthesizes the findings of heritage asset characterization and environmental exposure assessment to identify dominant degradation mechanisms and structurally vulnerable zones. This stage does not introduce new datasets but integrates previously compiled documentation, material characteristics, and environmental stressors to establish cause–effect relationships. The objective is to determine whether wind-driven phenomena contribute significantly to material deterioration and to define the analytical requirements of the physics-based modeling stage. Vulnerability identification focuses on elements exposed to aerodynamic loading, moisture accumulation, pollutant deposition, or localized flow acceleration. Particular attention is given to façade orientations, roof edges, protruding architectural features, and zones influenced by surrounding urban morphology.

Based on this evaluation, the analytical scope of the CFD simulation is defined. This includes the selection of representative wind directions, inflow velocity ranges, turbulence modeling approach, spatial resolution requirements, and the specific performance indicators to be extracted. The outcome of this stage is a clearly bounded numerical problem aligned with observed vulnerabilities, ensuring that the simulation targets physically meaningful degradation drivers rather than performing generic aerodynamic analysis.

3.5. Physics-Based Modeling (CFD)

The physics-based modeling stage quantifies wind-induced aerodynamic loading around the CHBS using computational fluid dynamics analysis. Direct simulation of erosion processes is not currently adopted in RADAR due to scale disparity and multi-physics complexity. Instead, wind flow behavior is resolved and interpreted as a proxy for degradation potential.

3.5.1. 3D Reconstruction

A three-dimensional model of the CHB and its surrounding terrain is generated from available geometric sources, including architectural drawings, historical documentation, Geographic Information System (GIS)/Digital Elevation Model (DEM) data, laser scanning, or Building Information Models (BIM). Geometric detail is preserved for elements influencing airflow separation, rainfall impingement, and pressure gradients, while non-critical architectural features are simplified to ensure computational efficiency. Domain dimensions for the analysis should comply with established best-practice guidelines [39–42]. The surrounding terrain extends at least $15H$ for multi-directional studies or $5H$ in upwind and lateral directions for single-direction analyses, with vertical clearance of at least $5H$. Blockage ratios shall also remain below recommended thresholds.

3.5.2. Mesh Generation

The computational domain is discretized using a volumetric computational mesh with local refinement near building surfaces to resolve boundary layer effects and surface pressure gradients. Surface discretization captures curvature and sharp geometric transitions where aerodynamically relevant. Mesh quality is assessed using standard metrics such as skewness, aspect ratio, and orthogonality. A grid independence study is conducted to ensure that key outputs, including pressure and wall shear stress distributions, are insensitive to further mesh refinement.

3.5.3. Boundary Conditions

Boundary conditions are defined according to environmental exposure data. Inlet profiles specify representative wind speed distributions, direction, and turbulence characteristics. The remaining domain boundaries are configured to minimize artificial confinement

effects and support physically realistic flow development. Terrain roughness parameters are incorporated to represent ground influence, and appropriate wall boundary conditions are applied to building surfaces.

3.5.4. CFD Simulation Setup

Wind flow is solved using an appropriate CFD approach selected in accordance with the study objectives, scale, and computational constraints. The selected turbulence model is chosen based on established performance in urban wind studies. Near-wall effects are represented using wall-resolved or wall-modeled approaches, as appropriate. Convergence is evaluated through residual monitoring and stabilization of integrated aerodynamic quantities. Verification and sensitivity assessment are performed where appropriate. Where possible, results are compared against established benchmarks, reference cases, or published validation studies for similar external flow configurations.

The primary outputs of this stage include wind velocity fields, surface pressure distributions, wall shear stress maps, and flow recirculation patterns, which form the quantitative basis for subsequent risk indicator integration.

3.6. Risk Indicator Integration

The risk indicator integration stage converts raw CFD outputs into physically interpretable degradation proxies. Rather than treating aerodynamic quantities as isolated numerical results, this stage systematically translates pressure distributions, wall shear stress values, and flow patterns into spatially meaningful exposure indicators linked to material vulnerability. Surface pressure fields are analyzed to delineate pressure zones characterized by elevated positive loading or suction effects. These regions may indicate increased susceptibility to wind-driven rain impingement, mechanical stress, or localized material detachment. In parallel, wall shear stress distributions are evaluated to identify areas subjected to sustained tangential aerodynamic forces, which may contribute to abrasion, surface wear, or enhanced pollutant deposition over time.

Flow recirculation zones are extracted from velocity field analysis to detect regions prone to pollutant accumulation and uneven moisture drying. By combining pressure behavior with flow stagnation characteristics, zones with increased moisture retention potential are identified, particularly where material properties suggest sensitivity to hygroscopic or salt-related degradation mechanisms. To ensure comparability across heterogeneous aerodynamic metrics, individual indicators are normalized using relative scaling procedures. This enables balanced evaluation without disproportionate influence from any single parameter. Finally, normalized indicators are spatially combined through multi-parameter overlay techniques, generating composite exposure maps that highlight zones where multiple degradation drivers coexist. These integrated risk layers provide the analytical foundation for the subsequent zone-based assessment stage.

3.7. Zone-Based Assessment and Decision Support

The zone-based assessment stage translates integrated risk indicators into spatially differentiated vulnerability zones that support conservation prioritization. Composite exposure maps derived from multi-parameter overlays are classified into relative vulnerability categories, reflecting the intensity and coexistence of degradation drivers.

Areas exhibiting concurrent high pressure loading, elevated wall shear stress, persistent recirculation, and increased moisture retention potential are categorized as high-vulnerability zones. Moderate and low-vulnerability zones are defined based on reduced indicator overlap or isolated exposure mechanisms. This classification enables clear spatial differentiation of risk intensity across façades, roof elements, and architecturally sensitive features. For each identified zone, dominant degradation drivers are explicitly associated

with the corresponding aerodynamic and environmental mechanisms. This linkage provides interpretability, allowing conservation specialists to distinguish whether deterioration risk is primarily driven by mechanical stress, abrasion potential, moisture accumulation, or pollutant deposition.

The resulting vulnerability zoning framework supports targeted, minimally invasive intervention strategies. By grounding conservation planning in physics-based exposure quantification and integrated indicator assessment, the RADAR methodology facilitates transparent, evidence-based decision support adaptable to diverse cultural heritage contexts.

4. Castle of Mytilene: A Real RADAR Use Case Scenario

To evaluate the efficacy of the innovative framework, the island of Mytilene, Greece, was selected as the testing ground. Mytilene is situated in the northeastern Aegean Sea, boasts a Mediterranean climate characterized by mild, wet winters and warm, dry summers. In particular, it is classified as "Csa" according to the Köppen–Geiger climate classification, which falls within the temperate (C) climate group, one of the five main global climate categories (A: tropical, B: arid, C: temperate, D: continental, E: polar), and is characterized by hot, dry summers and mild, wet winters [43]. The primary case study within Mytilene is the historic castle of Mytilene, a captivating emblem of the island's rich heritage. Detailed insights into the castle will be unveiled in the forthcoming section, while the results generated by the RADAR framework will be comprehensively presented, shedding light on its utility and applicability in safeguarding CHBS.

4.1. The Castle of Mytilene: Heritage Site Description and Restrictions

The Castle of Mytilene is located on the Greek island of Lesvos in the North Aegean and constitutes one of the largest fortified complexes in the Mediterranean, covering approximately 240,000 m^2 (Figure 4). The monument occupies a strategic hill between the northern and southern ports of Mytilene and was constructed upon the remains of the ancient acropolis of the city.



Figure 4. Mytilene castle overview from Google Maps.

Following the decline of its military function in the late Ottoman and early modern periods, the castle experienced gradual functional transformation and partial abandonment. In the 20th century, the monument was officially designated as a protected cultural

heritage site under Greek legislation and is currently managed by the Hellenic Ministry of Culture and Sports. Today, the site is partially accessible to visitors and exhibits heterogeneous conservation conditions. While stabilization and restoration interventions have been undertaken in selected areas, other zones present visible material weathering, surface erosion, biological colonization, and localized structural degradation. This spatial variability in preservation state makes the monument suitable for exposure-driven risk assessment within the RADAR framework [44].

The primary construction material of the castle is the so-called "Mystegna stone", sourced from the settlement and quarry of Mystegna in the eastern part of the island. According to the Directory of Greek Ornamental and Structural Stones of the Hellenic Geological and Mineral Exploration Authority [45]. Mystegna stone is an ignimbrite, a consolidated volcanic pyroclastic deposit formed from high-temperature ash and pumice flows. It is characterized by a density of approximately 2300 $kg\,m^{-3}$ and low porosity (3.8%). Its mineralogical composition includes albite–sanidine, orthoclase, phlogopite, biotite, and tosudite. The material properties of ignimbrite, particularly its response to moisture transport, salt crystallization, and surface abrasion, are directly relevant to the environmental exposure mechanisms analyzed in the present study.

4.2. Heritage Asset Characterization

This stage establishes the structural, material, and regulatory baseline of the Castle of Mytilene. It defines the physical properties of the monument, identifies its primary construction materials, and outlines the historical and legal constraints governing intervention and data acquisition. This characterization provides the contextual foundation required for subsequent environmental exposure analysis and physics-based modeling.

4.2.1. Documentation

The Castle of Mytilene constitutes a large-scale coastal fortification complex exposed to marine and aeolian environmental conditions. The documentation phase focused on collecting geometric, photographic, and contextual data necessary to characterize the structure and its surroundings. Archival information, publicly available imagery, and digital elevation data were used to reconstruct the spatial configuration of the monument and identify exposure-relevant features such as wall orientation, elevation differences, and proximity to the sea. The documentation process also included the systematic recording of observed deterioration patterns from publicly accessible sources. These observations were not used diagnostically but served as contextual reference points for later correlation with environmental and aerodynamic exposure indicators. This stage established the geometric and contextual baseline required for subsequent material assessment and environmental exposure analysis.

4.2.2. Material Identification

The castle is primarily constructed of natural stones and mortars whose durability depends strongly on mineralogical composition, porosity, and exposure orientation. Material performance is not spatially uniform. Wall orientation, elevation, and proximity to the ground significantly influence deterioration rates.

Major degradation mechanisms relevant to the case study include soluble salt crystallization, biogenic growth, marine aerosol deposition, and abrasion by wind-blown particles. Wind-driven processes are particularly critical in coastal environments. Aeolian transport contributes to surface abrasion, salt deposition, and alveolization, a weathering form characterized by cavity formation on stone surfaces. Studies have demonstrated that particle transport distance increases proportionally with wind speed and inversely with

grain size [46]. Abrasion damage is typically more intense near wall bases due to particle rebound dynamics [47].

Visual weathering classification methods, such as those proposed by Fitzner and Heinrichs, provide a framework for decay assessment; however, they rely on subjective interpretation [48]. For this reason, within the RADAR framework, material identification is combined with physics-based exposure indicators to reduce interpretative bias.

4.2.3. Historical and Regulatory Constraints

The Castle of Mytilene is protected under national heritage legislation, and any direct intervention, invasive inspection, or drone-based geometric acquisition requires formal authorization from the Greek Ministry of Culture. These regulatory constraints limit the availability of high-resolution LIDAR surveys and in situ long-term environmental monitoring data. Furthermore, the monument has undergone multiple historical phases, including seismic events, war-related damage, restoration interventions, and structural modifications. These factors introduce uncertainty in attributing current deterioration exclusively to present environmental conditions. Consequently, the RADAR framework is applied primarily as a risk-screening and exposure assessment tool rather than as a predictive structural diagnosis mechanism.

4.3. Environmental Exposure Analysis

Historical meteorological data were obtained via publicly accessible Application Programming Interfaces (APIs), covering a 15-year period (2007–2022) with hourly resolution [49]. The statistical summary of temperature, humidity, wind speed, wind direction, rainfall, and snowfall is presented in Table 2.

Table 2. Statistical analysis of weather data.

	Temp (°C)	Humidity (%)	Wind Speed (m/s)	Wind Direction (°)	Rain 1 h (mm)	Rain 3 h (mm)	Snow 1 h (mm)
count	198,444	198,444	198,444	198,444	22,470	18	42
mean	17.75	65.61	3.42	155.22	0.80	1.01	0.30
std	6.99	14.07	2.59	133.91	0.98	0.92	0.38
min	−3.76	3	0	0	0.1	0.19	0.1
25%	12.49	56	1.5	10	0.2	0.44	0.13
50%	17.43	67	3.1	150	0.42	0.755	0.16
75%	23.35	76	5.1	300	1.02	1	0.23
max	39.19	100	65.8	360	21.34	2.94	1.7

The dataset indicates a Mediterranean climate characterized by mild winters and warm summers. Temperature ranges from −3.76 °C to 39.19 °C, with an annual mean of 17.75 °C. Relative humidity averages 65.61%, with fluctuations between 3% and 100%. Wind speeds average 3.42 m/s, with extreme gusts reaching 65.8 m/s. Rainfall events are typically short in duration, with an average 1-h intensity of 0.80 mm.

Correlation analysis (Figure 5) shows generally weak linear relationships between variables, with the exception of a moderate negative correlation between temperature and humidity (−0.50). This inverse relationship reflects seasonal climatic behavior. Histograms and trend visualizations (Figures 6 and 7) confirm pronounced seasonal variability. The wind rose analysis integrated with rainfall intensity (Figure 8) reveals that intense rain events are predominantly associated with northerly winds. This directional coupling is critical for assessing wind-driven rain exposure on north-facing walls.

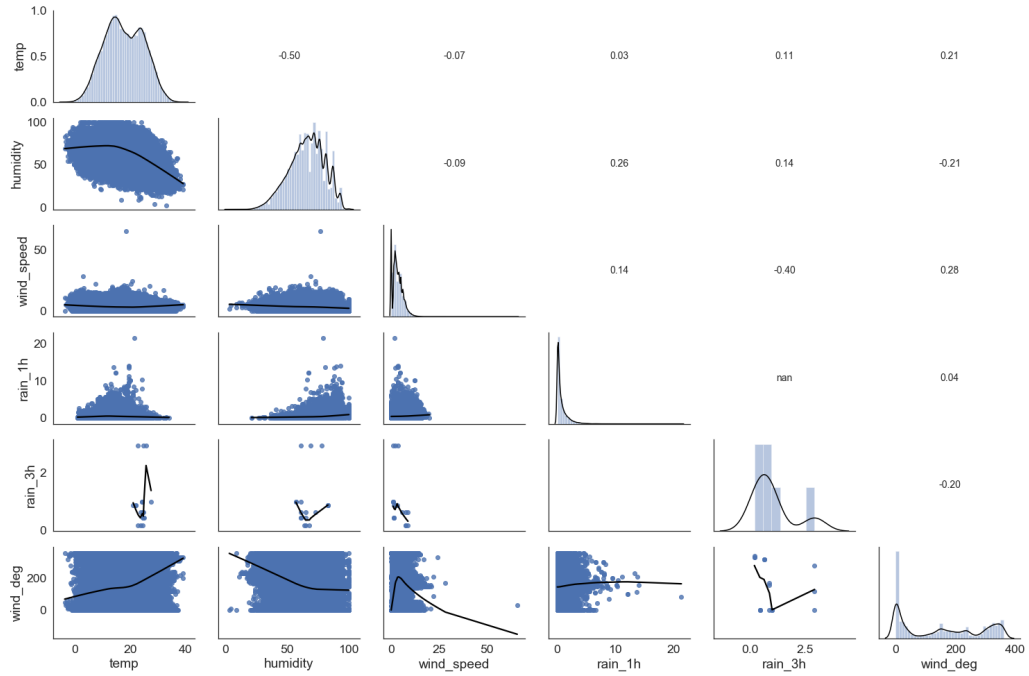


Figure 5. Correlation pair plot.

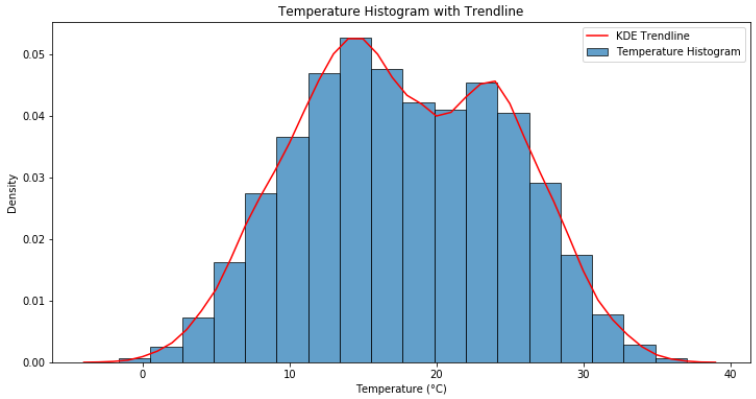


Figure 6. Temperature histogram with trendline.

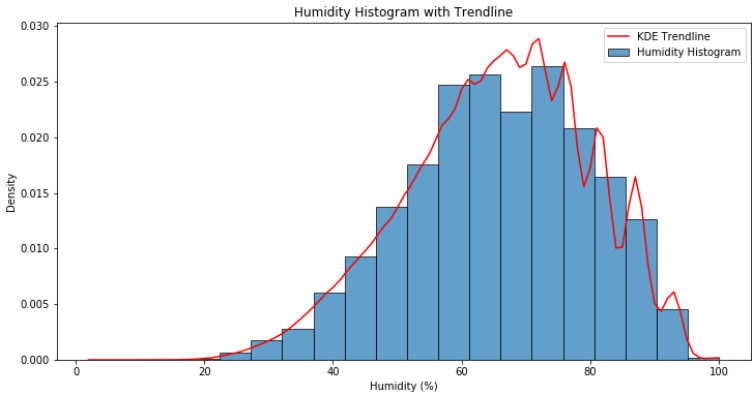


Figure 7. Humidity histogram with Kernel Density Estimation (KDE).

The combined interpretation of climatic parameters is summarized in Table 3. These findings provide the representative boundary conditions later applied in the CFD simulations and form the basis for exposure risk interpretation.

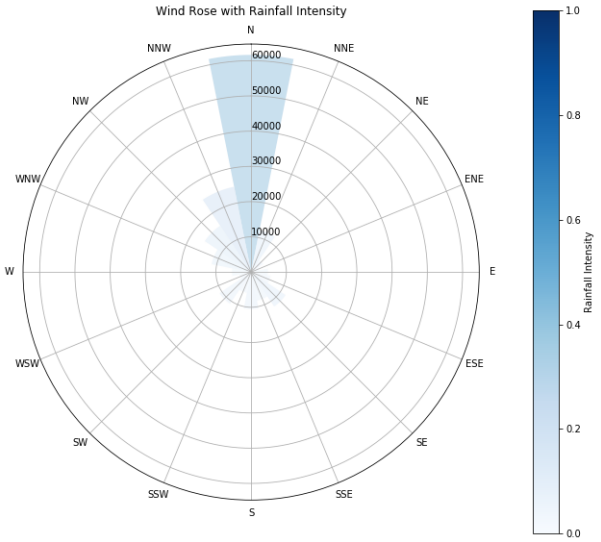


Figure 8. Wind Rose with Rainfall Intensity (1 h).

Table 3. Summary of Key Findings from Weather Data Analysis.

Aspect	Key Values	Implications
Temperature	Mean: 17.76 °C; Range: −3.76 °C to 39.19 °C	Significant seasonal variability; limited freeze–thaw risk but contributes to moisture transport mechanisms.
Relative Humidity (RH)	Mean: 65.62%; Range: 3% to 100%	Large fluctuations promote salt crystallization cycles and biological growth.
Wind Speed and Direction	Mean: 3.42 m s^{-1}; Max: 65.8 m s^{-1}; Predominantly N	North-originating winds associated with wind-driven rain and increased façade exposure.
Rainfall Patterns	1 h Mean Intensity: 0.80 mm; Short-duration events dominate	Episodic but intense moisture loading, especially under northerly winds.
Temperature–Humidity Correlation	$r = -0.50$	Inverse coupling affects drying potential and moisture persistence.
Impact on Cultural Heritage	Combined RH variability, wind-driven rain, particle deposition	Elevated risk of erosion, moisture ingress, salt damage, and surface weathering.

4.4. Condition Analysis and Analytical Scope Definition

The integration of material susceptibility and long-term environmental exposure data enables the identification of dominant deterioration drivers affecting the Castle of Mytilene. Documented visual records indicate spatially heterogeneous weathering patterns, including localized material loss and surface alteration. While direct in situ inspection was not conducted due to regulatory constraints, the consistency of observed patterns across independent visual sources supports their relevance for exposure risk interpretation.

Temperature variations in the region are moderate and abrupt freeze–thaw cycles are rare, suggesting that thermal stress is not the primary deterioration mechanism [50]. However, temperature fluctuations interact with relative humidity variability to facilitate internal moisture transport and salt crystallization cycles [51,52]. Relative humidity levels

fluctuating between 3% and 100% create favorable conditions for repeated salt crystallization and dissolution processes, contributing to progressive stone degradation.

Wind and wind-driven rain emerge as dominant external stressors. The wind rose analysis (Figure 8) demonstrates that intense rainfall events are predominantly associated with northerly winds. This representation allows the identification of dominant rain-bearing wind sectors, revealing that intense rainfall events are predominantly associated with northerly winds. This directional information is essential for assessing façade-specific exposure and cannot be inferred from descriptive statistics alone. This directional coupling indicates anisotropic exposure, where north-facing façades are subjected to increased wind-driven rain impingement and marine aerosol transport. Short-duration but intense rainfall events, combined with aerodynamic forcing, increase the likelihood of moisture ingress and surface erosion.

Table 4 summarizes the relationships between environmental parameters and material deterioration mechanisms. The correlations identified suggest three principal stress pathways: (i) pressure-driven moisture penetration during wind-driven rain events, (ii) tangential aerodynamic loading leading to particle-induced abrasion, (iii) prolonged moisture retention in zones with limited ventilation. These identified mechanisms define the analytical scope of the subsequent CFD simulations, which aim to quantify pressure distribution, wall shear stress, and airflow recirculation patterns under representative northerly wind conditions.

Table 4. Summary of environmental impacts on building materials.

Environmental Factor	Observation	Impact on Building Materials	Key Correlation
Temperature	Average 17.76 °C, range from −3.76 °C to 39.19 °C	Limited direct effect on material deterioration due to mild fluctuations	Fluctuations influence internal movement of aqueous solutions affecting salt crystallization cycles and biological growth.
Relative humidity	Average 65.62%, fluctuates from 3% to 100%	High fluctuations cause salt crystallization cycles, leading to material damage	High correlation with increased salt-induced surface damage, especially during low-temperature periods with high humidity.
Wind speed and direction	Average 3.42 m/s, gusts up to 65.8 m/s, mostly from north	Causes abrasion, deposition of marine aerosol, and wind-driven rain	Correlation between northward winds and increased rain, leading to heightened erosion and material degradation on exposed surfaces.
Rainfall	Average 1-h intensity of 0.80 mm	Short, intense rains cause infiltration and potential cracking	High correlation between intense rain events and increased erosion in wind-exposed regions, especially with northward wind patterns.
Airborne particles (PM1, PM2.5, PM10)	Concentration varies with industrial and traffic emissions; new particle species are produced by the reaction of sea-salt aerosol and particles deriving from fossil fuel combustion	Causes soiling, erosion, and chemical reactions on surfaces	Increased particle levels correlate with seasonal environmental stress, accelerating surface erosion and chemical weathering.

4.5. Physics-Based Modeling (CFD)

The physics-based modeling stage implements the analytical scope defined in the previous subsection by quantifying the aerodynamic mechanisms associated with wind-driven deterioration. Based on the identified dominant stress pathways, the CFD simulations aim to evaluate surface pressure distribution, wall shear stress, and airflow recirculation patterns under representative northerly wind conditions. These indicators provide spa-

tially resolved exposure metrics required for subsequent risk interpretation within the RADAR framework.

4.5.1. 3D Reconstruction

The three-dimensional reconstruction of the Castle of Mytilene and its surrounding terrain was performed using a combination of open-access geospatial datasets and photographic documentation. The terrain geometry was generated from a DEM obtained from the Copernicus database [53]. The DEM data were processed to create a heightmap, which was subsequently refined to mitigate resolution artifacts caused by the original 20 m elevation grid. The refined heightmap was imported into Blender to generate the terrain surface, followed by smoothing operations to ensure geometric continuity. Blender was selected due to its open-source architecture, robust mesh editing capabilities, support for STL export, and scripting flexibility, which facilitate reproducible geometry preprocessing without licensing constraints. Its suitability for terrain modeling and mesh refinement made it adequate for preparing the CFD-ready geometry. The adopted geometric workflow ensures aerodynamic representativeness sufficient for the objectives of the present RADAR application. While higher-resolution geometric acquisition (e.g., terrestrial laser scanning or LiDAR) may further refine localized flow predictions, such enhancements extend beyond the scope of the current framework validation and are considered part of future methodological developments.

The castle geometry was reconstructed through a hybrid workflow combining DEM information (20 m elevation resolution) and multi-angle photographic references. The perimeter layout of the walls was derived from elevation overlays, and vertical extrusion was applied to match documented wall heights. Manual refinements were introduced using photographic evidence to ensure geometric consistency with visible structural features. The adopted approach provides meter-scale geometric accuracy sufficient to capture the global morphology and aerodynamic envelope of the monument. In contrast, LiDAR-based acquisition or terrestrial laser scanning typically delivers centimetric or sub-centimetric precision and dense point clouds capable of resolving fine architectural details such as surface irregularities, crenellations, and small geometric discontinuities. Such high-resolution datasets would improve the representation of localized flow separation and micro-scale shear stress variations.

However, drone-based LiDAR surveys require special authorization from the Greek Ministry of Culture and are restricted in this case due to regulatory constraints. For the purposes of the present RADAR application, which focuses on exposure patterns at the building-envelope scale rather than conservation-detail resolution, the adopted geometric workflow ensures sufficient aerodynamic representativeness. Higher-resolution acquisition may further refine localized flow predictions and is considered a direction for future methodological refinement.

The reconstructed geometry was exported in STL format and further processed in Ansys SpaceClaim (v2023R1) to ensure watertight surfaces and eliminate inconsistencies such as non-manifold edges, foldovers, and self-intersections. The computational fluid domain was subsequently extracted from the cleaned geometry. Figure 9 presents the final domain dimensions, illustrating the extended upstream and downstream distances adopted to satisfy best-practice blockage ratio requirements and to allow proper development of the atmospheric boundary layer. The vertical extent of the domain ($15H$) ensures adequate representation of flow stratification above the highest castle elevation, while the horizontal offsets ($5H$–$10H$) minimize artificial boundary interference. Figure 10 illustrates the reconstructed 3D model of the castle and the defined surface regions used to facilitate meshing, boundary condition assignment, and post-processing. The subdivision into

distinct façade and terrain zones enables localized extraction of aerodynamic indicators, such as wall shear stress and pressure distributions, which are later integrated into the RADAR risk interpretation framework.

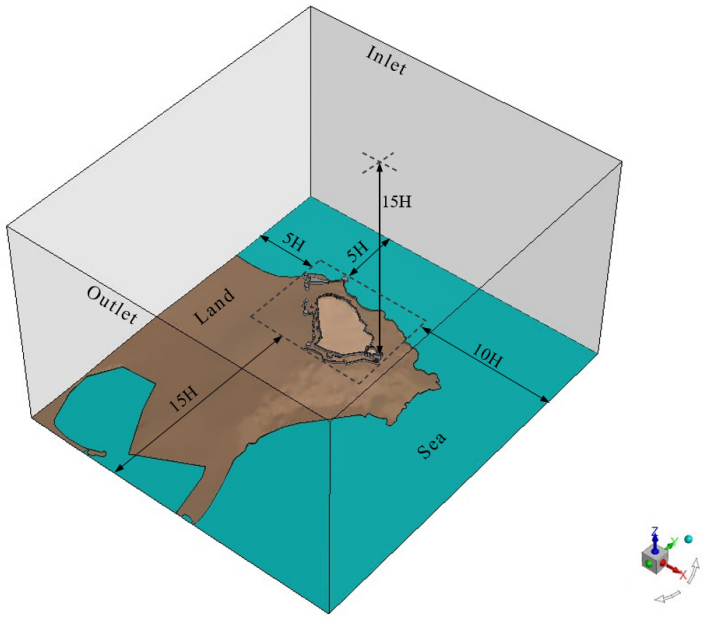


Figure 9. Domain dimensions.

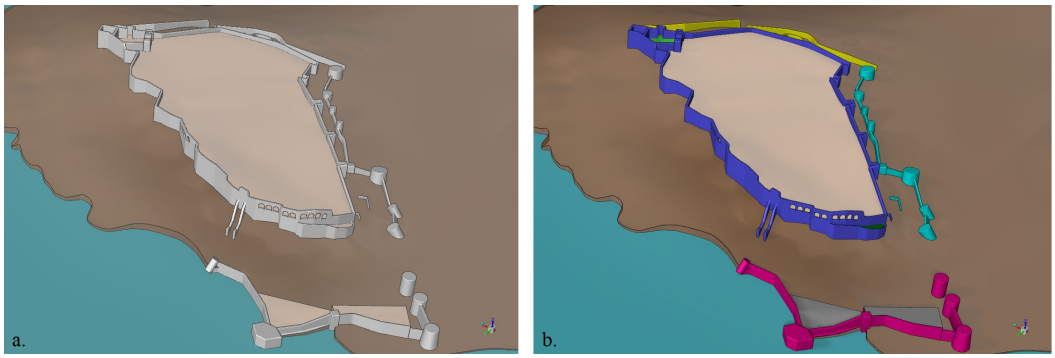


Figure 10. 3D model of the castle of Mytilene. (**a**) General view; (**b**) defined regions for ease of pre- and post-processing.

The domain extent was selected following established best-practice guidelines for pedestrian-level and urban-scale wind simulations [39–42,54,55]. In Figure 9, *H* denotes the vertical distance from the ground to the highest wall section (approximately 55 m). To satisfy blockage-ratio constraints and account for the mixed roughness conditions of the site (hilly terrain adjacent to low-roughness sea surface), offsets were extended beyond minimum recommendations, resulting in an overall blockage ratio of 2.77%. Consequently, the domain dimensions were set to 1500 m (north–south), 1320 m (east–west), and 880 m (vertical).

The computational mesh was created in Ansys Fluent Meshing v2023R1 using the Watertight geometry workflow. The polyhexcore meshing technique, also known as mosaic meshing, was utilized, combining polyhedral elements near complex boundaries with structured hexagonal cells in the interior domain to balance geometric fidelity and computational efficiency. Local sizing functions were applied to the different façade and terrain zones (Figure 10b), in combination with curvature and proximity refinement, ensuring at least five cells across the thickness of critical structural elements such as the castle walls (Figure 11). The boundary layer was resolved using six inflation layers applied to the

castle walls, land, and sea surfaces to capture near-wall velocity gradients and wall shear stress accurately.

Figure 11 illustrates the multi-scale discretization strategy adopted for the study. The detailed views highlight mesh refinement along wall edges, corners, and near-ground interfaces where flow separation and shear stress amplification are expected. The gradual transition toward coarser elements in the far-field region ensures computational efficiency without compromising resolution in areas critical for aerodynamic exposure assessment.

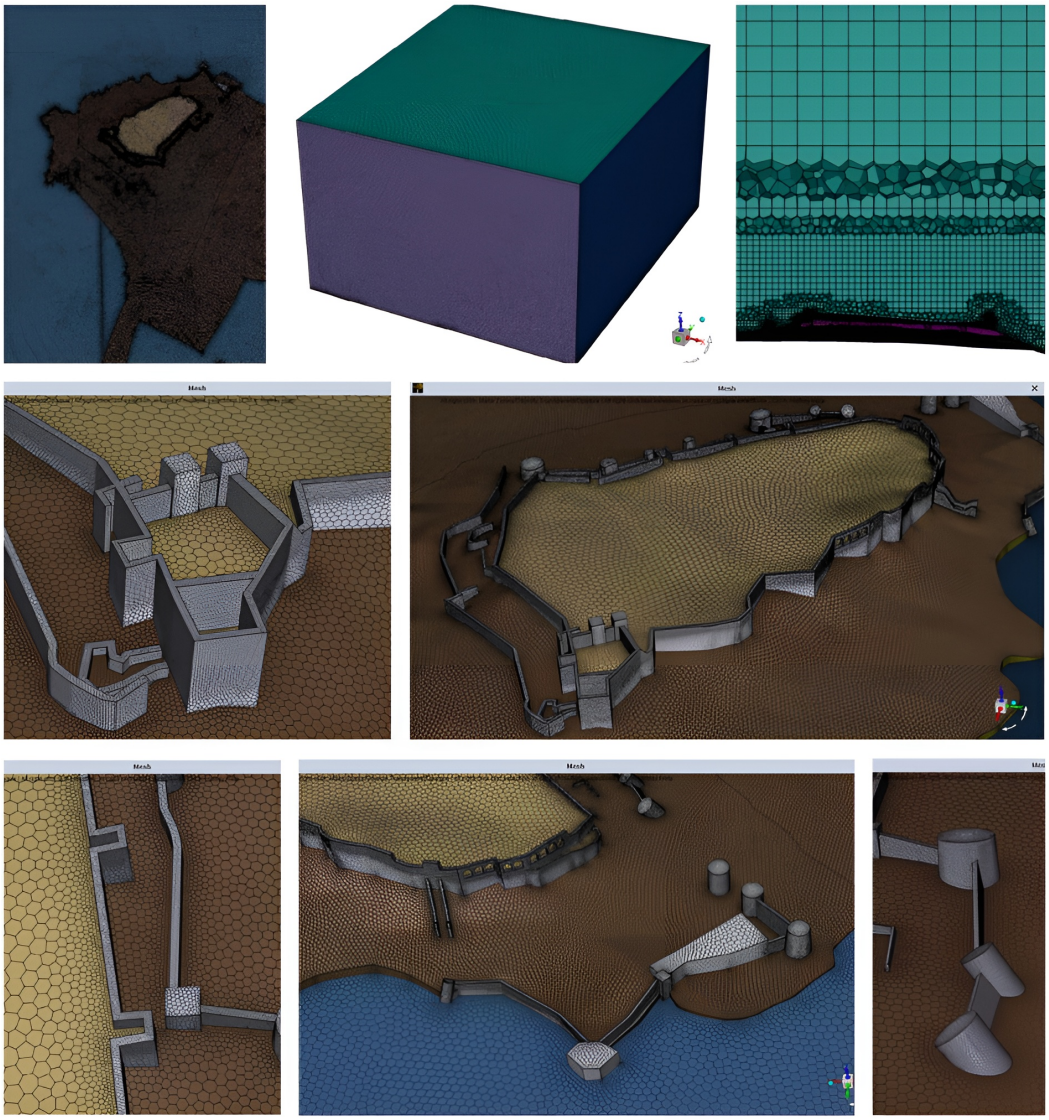


Figure 11. Computational mesh. Multiple views and sections.

As a result, a volume mesh was created with a total number of 3,659,493 elements and a minimum and average orthogonal quality of 0.275 and 0.940 respectively. Additionally, for verification purposes, a mesh convergence study was performed.

The geometric model was developed to represent the overall morphology and aerodynamic envelope of the castle rather than to reproduce architectural details at conservation-scale precision. Wall footprints were derived from DEM overlays and cross-checked with photographic documentation, while the vertical development (z-dimension) was generated through controlled extrusion to wall heights estimated from available topographic data and visual references. High-resolution UAV-based photogrammetry or LiDAR scanning was not feasible due to regulatory restrictions on aerial operations in the vicinity of the site, which is located near a military aviation zone. Such constraints are common in cultural

heritage environments. The adopted level of geometric detail was therefore defined to ensure aerodynamic representativeness and numerical stability, which are the primary requirements for environmental exposure assessment within the RADAR framework.

4.5.2. Boundary Conditions

- *Representative environmental conditions:* Based on the thorough environmental conditions analysis, the meteorological conditions from Table 3 were used as input data for the simulations.
- *Operating and initial conditions:* The initial and operating conditions for the simulations, as well as the material properties, were defined based on the representative environmental conditions.
- *Boundary conditions:* The locations of the inlet (north) and outlet (south) boundaries are presented in Figure 9 and they were defined as a velocity inlet and an outflow boundary (all gradients normal to the boundary are zero), respectively. At the velocity inlet, profiles variable with height were prescribed for velocity, turbulent kinetic energy and turbulent dissipation rate, acc. to [56–59], Equations (1)–(5).

$$U = \frac{u_*}{\kappa} \ln\left(\frac{z + z_0}{z_0}\right), \tag{1}$$

$$k = \frac{u_*^2}{\sqrt{C_\mu}}, \tag{2}$$

$$\varepsilon = \frac{u_*^3}{\kappa(z + z_0)}, \tag{3}$$

$$\omega = \frac{\varepsilon}{k\beta'} \tag{4}$$

$$\tau = \rho u_*^2 \tag{5}$$

In Equations (1)–(5), the following notation is used:

U—mean streamwise wind velocity [m/s];
u_*—atmospheric boundary layer (ABL) friction velocity [m/s];
κ—von Kármán constant (=0.41);
z—height above ground level [m];
z_0—aerodynamic surface roughness length [m];
k—turbulent kinetic energy [m^2/s^2];
C_μ—turbulence model constant (=0.09);
ε—turbulent dissipation rate [m^2/s^3];
ω—specific turbulent dissipation rate [1/s];
β'—model constant used in the k–ω formulation;
τ—driving shear stress [Pa];
ρ—air density [kg/m^3].

Domain lateral boundaries were modelled using the symmetry boundary condition. The selected domain size ensures that the flow is undisturbed by the non-physical domain boundaries. In order to fulfil the theoretical requirements for achieving horizontal homogeneity of the flow parameters in the atmospheric boundary layer, driving shear stress was assigned at the top layer of cells of the domain, Equation (5) [56–61], and at the ground and sea boundaries—a respective surface roughness corresponding to their relevant categories in the Wieringa roughness classification [62], ($z_{0,sea}$ = 0.0002 m and $z_{0,ground}$ took the values of 0 m, 0.1 m, and 0.5 m for the different ground areas with different roughness).

The castle structure was modelled using free-slip walls.

4.5.3. CFD Simulation Setup

The airflow around the Castle of Mytilene was simulated using a steady-state Reynolds-Averaged Navier–Stokes (RANS) approach. RANS modeling was selected due to its computational efficiency and its demonstrated suitability for resolving mean flow characteristics in outdoor and urban-scale wind simulations [42]. Given the objective of quantifying average aerodynamic exposure indicators rather than transient turbulence structures, steady-state RANS provides an appropriate balance between accuracy and computational cost.

The simulations were performed using Ansys Fluent v2023R1. Turbulence was modeled using the generalized k–ω (GEKO) model [63], which consolidates the advantages of the k–ϵ and k–ω families, combining freestream independence with robust near-wall performance. The GEKO model was employed with the wall-distance-free formulation, coefficients $C_{SEP} = 1$ and $C_{NW} = 1$, and a production limiter clip factor of 10 to prevent excessive turbulence buildup in stagnation regions without affecting calibrated flow behavior.

Pressure–velocity coupling was handled using a coupled scheme to enhance numerical stability and convergence speed. Second-order spatial discretization schemes were applied for pressure, momentum, turbulent kinetic energy, and specific dissipation rate. Double precision arithmetic was employed to improve numerical accuracy.

Convergence was assessed through residual monitoring and stability of surface-integrated quantities. Residuals for velocity dropped below 10^{-8}, while continuity, turbulent kinetic energy, and specific dissipation rate residuals decreased below 10^{-6}. Additionally, surface pressure and wall shear stress values on the castle envelope were monitored and exhibited stable asymptotic behavior, indicating solution convergence.

4.5.4. Verification and Validation

The verification activities performed to ensure the model's fidelity are briefly summarized in the following paragraphs.

- *Grid independence study*

For the grid sensitivity analysis, 3 different discretization schemes were tested with different mesh sizes and refinements. The cell sizes for the different regions are varied by a factor of 1.5 between the three meshes. Additionally, the castle walls are discretized with 4, 5, and 6 cells for the meshes denoted as coarse, medium and fine, respectively. The number of cells for the different resolutions corresponds to 1,855,995, 3,659,493, and 7,749,500 volumetric cells for the three grids.

A general view of the visual comparison between the meshes in the castle area is presented in Figure 12. The medium mesh was selected as the basis for further simulations based on a balance of computational efficiency and resolution accuracy. To support this choice a comparative analysis of wall shear stress across the three meshes was performed. Although the distribution of stresses throughout the castle walls was qualitatively similar, the relative differences between the medium and coarse were not negligible. On the other hand, the medium mesh displayed a satisfactory convergence of results with only marginal deviations compared to the fine mesh, indicating that further refinement would not significantly affect the solution accuracy. Contour plots of the relative percentage differences in wall shear stress between the medium and coarse meshes and between the medium and fine meshes are presented in Figure 13a,b.

Due to the nature and the goals of the current study, namely erosion prediction, for the purposes of grid sensitivity analysis, only the results for the shear stress parameter on the castle walls are discussed here.

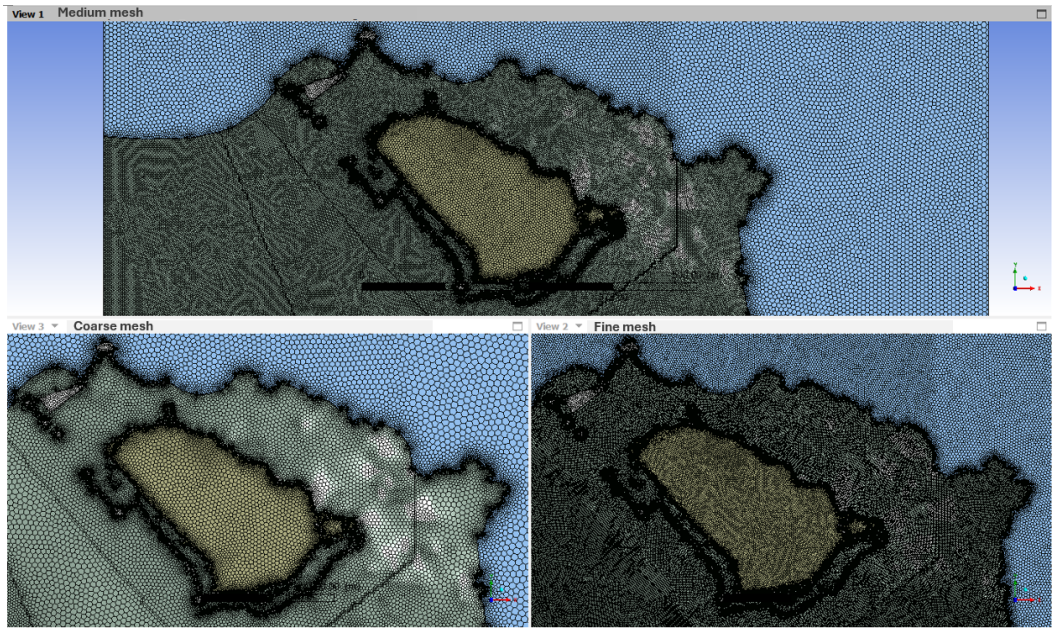


Figure 12. Medium (**top**), coarse (**bottom left**) and fine (**bottom right**) mesh—castle area general view.

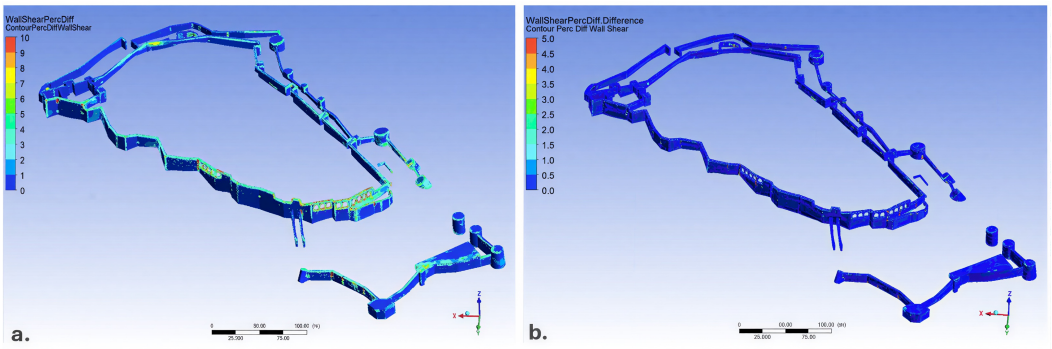


Figure 13. Wall shear stress relative percentage differences: (**a**) between medium and coarse mesh; (**b**) between medium and fine mesh.

- *Horizontal homogeneity of the flow*

Horizontal homogeneity of the flow through the computational domain is a fundamental factor for ensuring the reliability of any CFD analysis related to modeling wind flow in the atmospheric boundary layer. The study for the castle of Mytilene was performed in an empty domain, discretized with a mesh, corresponding to the "medium mesh" described in the previous paragraph. Horizontal homogeneity was evaluated by examining the uniformity of key flow parameters (wind velocity, turbulence intensity (TI), turbulent kinetic energy (TKE), and turbulent specific dissipation rate (TSDR)) across several vertical sections within the domain. These were strategically positioned at different locations, see Figure 14, to comprehensively capture the development of the wind profiles throughout the whole domain. Three rows of lines at 5 y-coordinates each were defined in the middle of the castle geometry and its most westward and eastward sides. Line notations follow the format *line-i-j*, where index "*i*" takes values "*w*", "*m*", and "*e*" corresponding to the west, middle, and east locations in the x-direction, and index "*j*" varies from 1 to 5 (1 coinciding with the y-coordinate of the inlet, increasing to 5 at the outlet boundary).

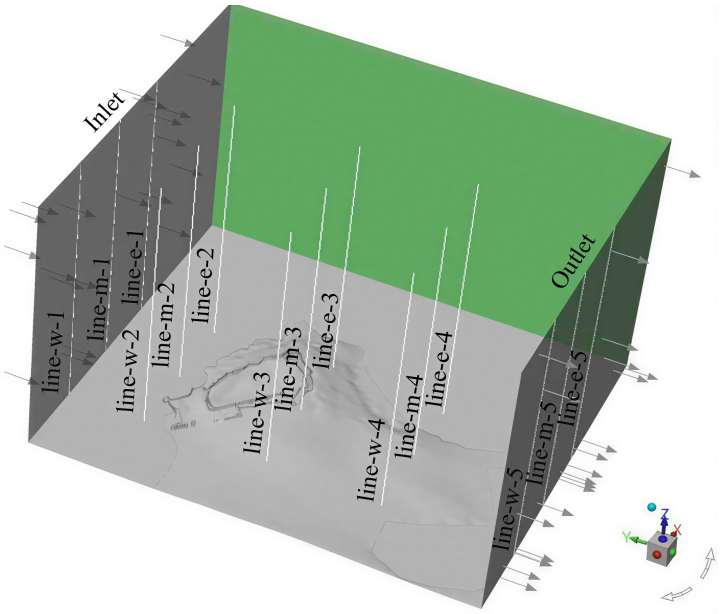


Figure 14. Locations and notations of the vertical sections for flow horizontal homogeneity analysis. Arrows show wind flow direction.

The vertical profiles of velocity, turbulent kinetic energy, and specific dissipation rate distribution with height at the different locations are presented in Figure 15.

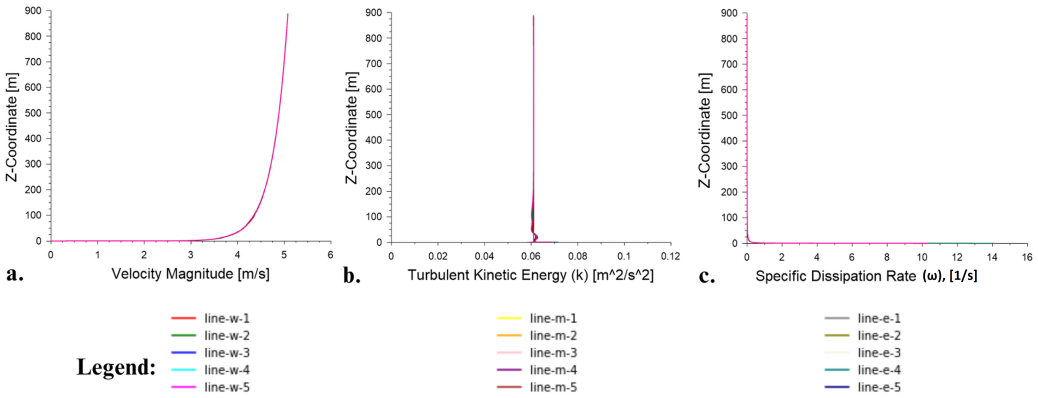


Figure 15. X-Y plots of: (**a**) velocity distribution; (**b**) turbulent kinetic energy distribution; (**c**) specific dissipation rate distribution with height.

The maximum deviations between each group of curves (representing the flow parameter variations from the inlet to the outlet) were below 0.8% for the velocity parameter, 1.2% for TI, 2.5% for TKE, and 12% for TSDR. These results were considered sufficient for ensuring the key flow parameters and inlet profiles remain unchanged across the empty domain, suggesting that the flow in the model with the actual geometry would develop appropriately without artificial disturbances from the computational setup.

Quantitatively validating the CFD results was not possible due to the absence of long-term, in situ data, and the monument's complex history of seismic events, war damage, alterations and restoration activities over its lifetime. The simulations were therefore evaluated through a qualitative, physics-based consistency assessment, focusing on the relative spatial distribution of exposure patterns. The zones of the castle walls exhibiting active deterioration (such as biological colonization or surface deterioration) were viewed as a form of contextual evidence for sustained micro-climate stress. Conversely, well-preserved or restored areas were not considered informative of exposure conditions. Historical photographs and contemporary publicly available imagery were utilized to gather contextual

information on observed material condition and only to document consistent patterns of deterioration, rather than to establish causal relationships. Based upon this documentation the CFD model results were used to determine those locations that are experiencing increased levels of environmental exposure, and correspondingly, increased conservation demands as determined by the RADAR assessment (Table 5), supporting their use for risk screening rather than for diagnostic or predictive purposes [64]. Two examples of such comparisons are presented in Figures 16 and 17.

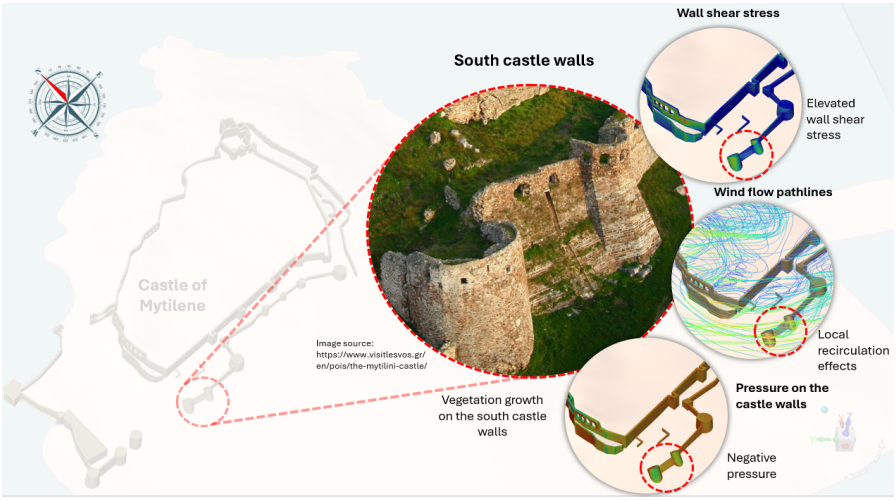


Figure 16. South castle walls—CFD analysis results and contextual photograph from site. In the adopted color maps, the blue range indicates lower values of the visualized parameter, whereas the red range indicates higher positive values.

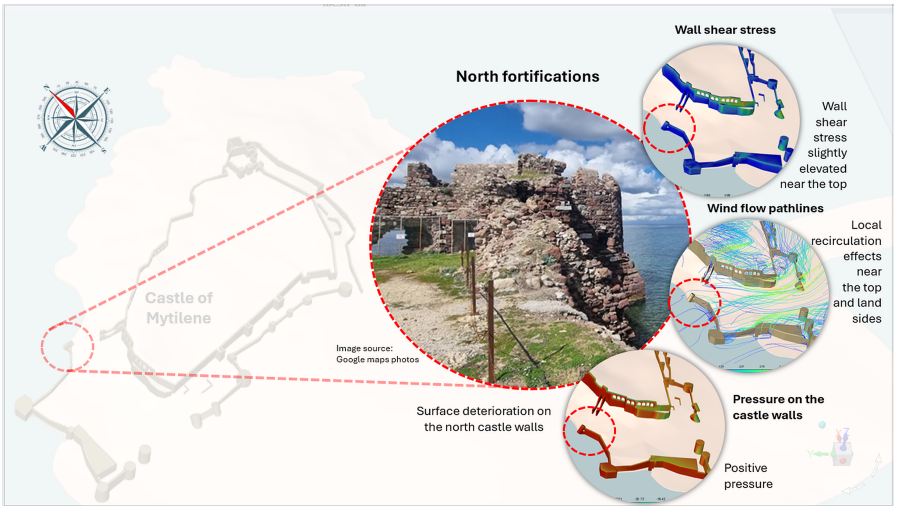


Figure 17. North castle walls—CFD analysis results and contextual photograph from site. In the adopted color maps, the blue range indicates lower values of the visualized parameter, whereas the red range indicates higher positive values.

4.5.5. Castle of Mytilene: Simulation Results

The wind flow simulations around the Castle of Mytilene yield critical insights into the aerodynamic forces acting on the historical structure. Key among these insights are the distributions of pressure and wall shear stress, and the visualization of pathlines, which together offer a comprehensive understanding of the potential erosion patterns influenced by wind flow.

- *Wall shear stress (WSS)*
  Wall shear stress provides an indicator of the tangential mechanical forces exerted

by the wind along the surface of the castle envelope. Areas of high WSS correlate with potential zones of accelerated surface-level material wear and erosion-related processes, as they reflect intensified near-wall velocity gradients and shear loading. Through the CFD simulation, the surface of the castle was mapped based on the WSS values, see Figure 18. This heatmap can later be used by CHBS conservation specialists for identifying the regions where the WSS values exceed the threshold that materials constituting the castle walls are known to withstand over time. Furthermore, it can show areas endangered by surface abrasion, particle removal or adhesion, erosion of fragile material layers, and localized modulation of biological growth.

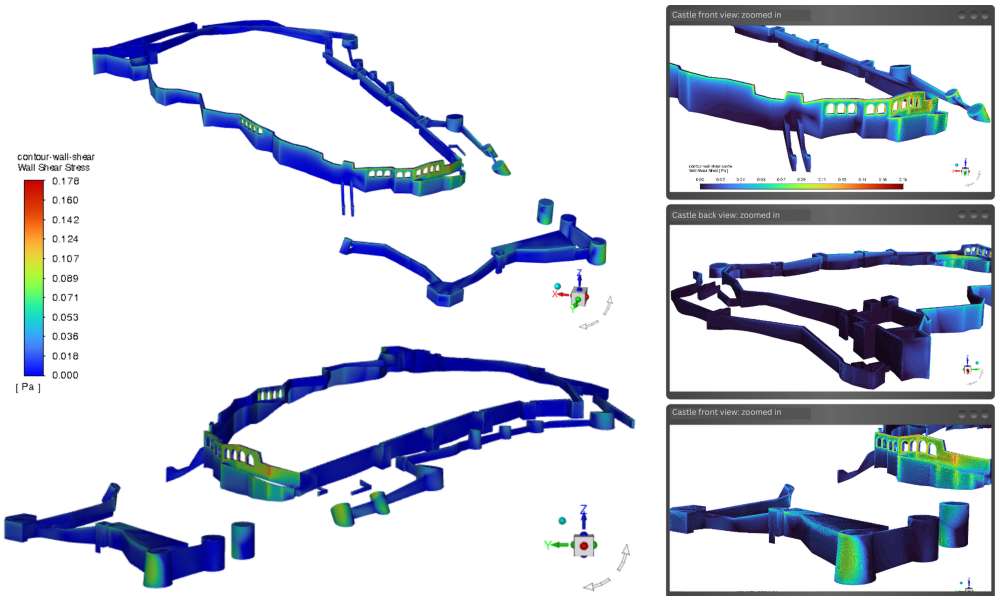


Figure 18. Wall shear stress contour plot on castle walls.

- *Pressure on walls*
  While WSS reflects the tangential forces exerted by the flow on the wall surfaces, the distribution of static pressure represents the normal aerodynamic loading acting on the structure. In this field, pressure maxima are associated with flow deceleration and stagnation at windward surfaces, and pressure minima are mainly resulting from flow acceleration and separation in leeward and sheltered regions. Static pressure distribution (relative to the ambient environmental pressure) for the castle of Mytilene subjected to the identified median north wind is presented in Figure 19.
- *Wind flow pathlines visualization*
  Pathline visualization complements the WSS and pressure analysis by tracing the trajectories of particles carried by the wind, offering a dynamic representation of the airflow structure around the castle. Figure 20 presents the overall flow field under representative northerly wind conditions, highlighting acceleration zones along exposed windward walls and pronounced flow deflection over elevated perimeter sections. Large-scale recirculation regions are visible in the leeward and recessed areas of the fortress, indicating zones of reduced ventilation and prolonged residence time of airborne moisture and particles. Figure 21 provides detailed views of localized flow phenomena near architectural discontinuities, such as corners, towers, and wall bases. These regions exhibit vortex formation, flow separation, and shear layer development, which are directly associated with intensified particle deposition, salt accumulation, and potential surface abrasion. The observed flow patterns therefore support the identification of spatially differentiated deterioration mechanisms within the RADAR framework.



Figure 19. Static pressure distribution.

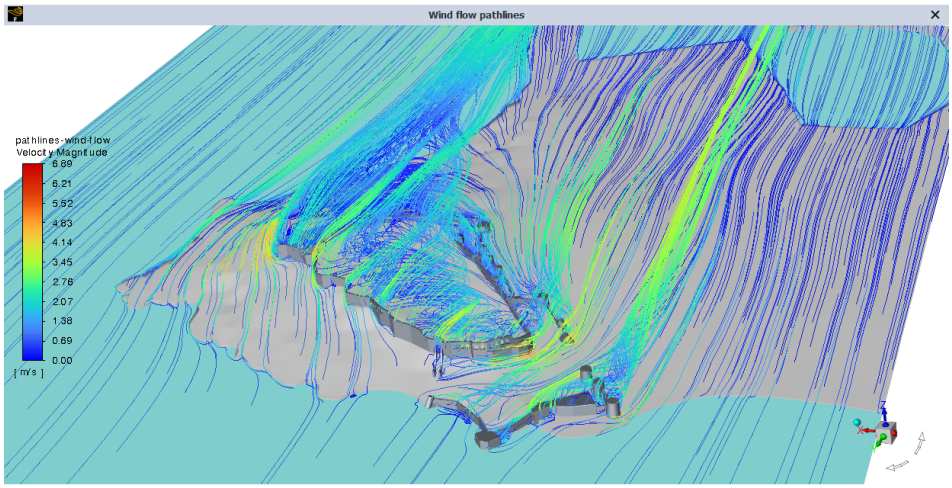


Figure 20. Windflow pathlines—general view.

4.6. Risk Indicator Integration

This stage integrates the environmental exposure analysis with the CFD-derived aerodynamic indicators to generate spatially resolved risk descriptors. The objective is not to restate raw numerical outputs, but to translate pressure distribution, wall shear stress, and airflow recirculation patterns into interpretable conservation-relevant indicators.

Environmental monitoring (Tables 3 and 4) revealed persistent relative humidity fluctuations, recurrent northward wind-driven rain events, and episodic high wind speeds. These background climatic stressors provide the exposure context within which aerodynamic amplification mechanisms operate.

The CFD results quantify how this exposure context interacts with the geometry of the Castle of Mytilene. Static pressure distribution (Figure 19) identifies zones of normal aerodynamic loading associated with windward stagnation regions. These areas are susceptible to wind-driven rain impingement and pressure-driven moisture ingress through porous materials and joints. Conversely, low-pressure leeward regions indicate sheltering but may coincide with reduced ventilation capacity.

Wall shear stress (Figure 18) captures tangential aerodynamic forcing and therefore highlights zones vulnerable to abrasion, particle detachment, and mechanical surface

degradation. Elevated WSS values are primarily concentrated along exposed edges, corners, and upper elevations where flow acceleration occurs.

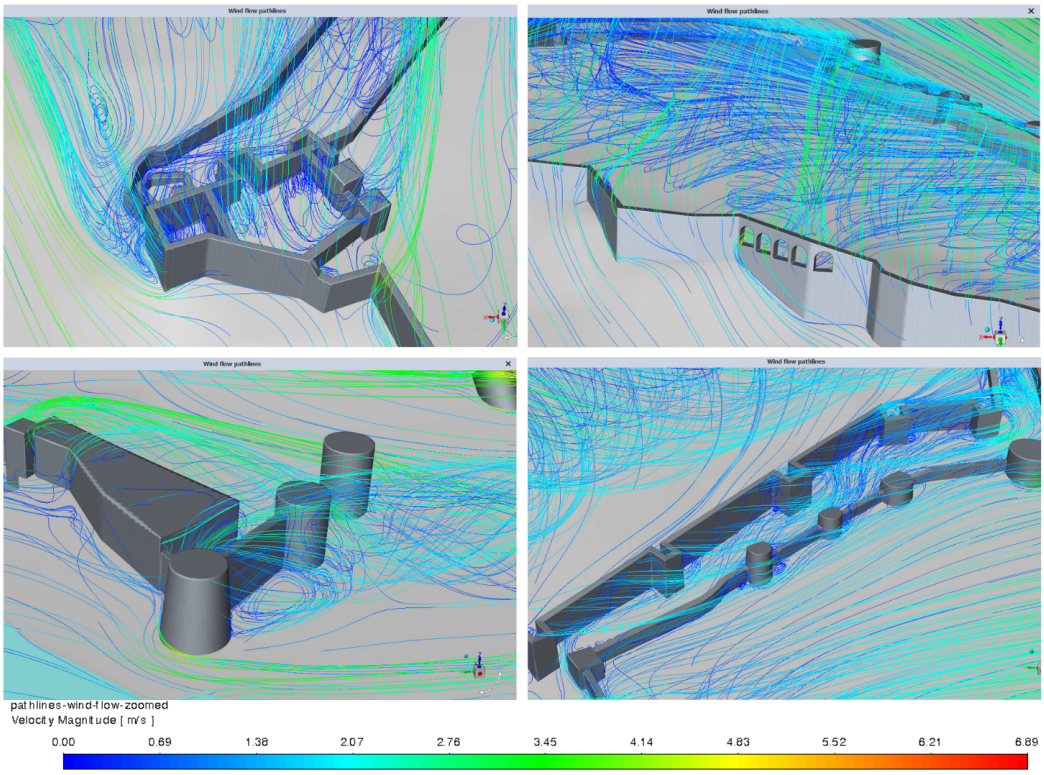


Figure 21. Windflow pathlines—detail views.

Pathline visualization (Figures 20 and 21) complements these indicators by revealing recirculation zones and low-velocity regions. These areas are characterized by reduced air exchange and prolonged moisture residence time, increasing susceptibility to salt crystallization, biological colonization, and long-term material fatigue.

To enable structured interpretation, the aerodynamic outputs were normalized and overlaid with environmental exposure parameters, producing composite exposure zones. This multi-parameter overlay approach allows the distinction between pressure-dominated infiltration pathways, shear-dominated erosion mechanisms, and recirculation-driven moisture retention zones.

The integrated risk indicators serve as the analytical input for the subsequent zone-based assessment stage, where spatial prioritization and condition categorization are performed.

4.7. Zone-Based Assessment

Based on the integrated aerodynamic indicators and environmental exposure parameters described in the previous subsection, a spatially differentiated assessment of deterioration risk was performed. The objective of this stage is to translate quantitative exposure metrics into operational conservation categories, enabling targeted and non-invasive intervention planning.

The combined evaluation of static pressure, wall shear stress, airflow recirculation behavior, and background climatic stressors reveals that deterioration mechanisms are not uniformly distributed across the castle envelope. Instead, risk intensity is strongly governed by orientation, elevation, and geometric discontinuities such as edges, corners, recessed façades, and near-ground zones.

Table 5 summarizes the zone-based RADAR assessment, identifying dominant environmental drivers, CFD-identified aerodynamic behavior, and the resulting condition interpretation for each spatial category.

Table 5. RADAR-based condition assessment of the Mytilene castle zones.

Assessed Zone	Dominant Environmental Exposure	CFD-Identified Behavior	Condition Assessment
Zone 1 North-facing exposed walls	High wind speeds (avg. 3.42 m/s, gusts up to 65.8 m/s), wind-driven rain	High static pressure gradients and localized flow acceleration	Elevated risk of surface erosion, abrasion, and moisture penetration due to wind-driven rain
Zone 2 Leeward and recessed areas	Persistently high relative humidity (up to 100%), low drying potential	Flow separation and recirculation zones	High risk of moisture accumulation, salt crystallization, biological growth, and surface degradation
Zone 3 Elevated perimeter sections	Large temperature range (−3.76 °C to 39.19 °C), RH variability	Pressure fluctuations and flow channeling	Cyclic thermal–hygrometric stress promoting internal moisture transport and material fatigue
Zone 4 Near-ground and sheltered areas	Deposition of airborne particles (marine aerosol, PM1–PM10)	Low-velocity flow and particle deposition/accumulation	Increased surface soiling, chemical weathering, and long-term material decay
Zone 5 Wind-exposed corners and edges	Combined wind, rain, and RH fluctuations	Localized pressure concentration and turbulence	Synergistic deterioration mechanisms, including cracking, erosion, and accelerated aging

The assessment demonstrates that north-facing and directly exposed surfaces are primarily governed by infiltration-driven and erosion-driven mechanisms, while leeward and recessed areas are dominated by moisture-retention pathways. Near-ground regions exhibit enhanced particle accumulation due to reduced flow velocities, increasing long-term chemical weathering potential. Importantly, the RADAR framework does not prescribe uniform conservation measures. Instead, it enables spatial prioritization and mechanism-specific mitigation strategies. Pressure-dominated zones require rain-shielding and drainage optimization, shear-dominated regions may benefit from protective surface treatments, and recirculation-prone areas demand ventilation-aware preservation planning.

This structured zone-based evaluation transforms aerodynamic simulation outputs into actionable conservation intelligence, supporting preventive maintenance, monitoring prioritization, and resource-efficient heritage management.

5. Discussion

The present study introduced RADAR as a structured, non-invasive framework for environmental risk assessment of cultural heritage buildings and structures, integrating environmental exposure analysis with physics-based CFD modeling and zone-based interpretation. The case study of the Castle of Mytilene enables a critical evaluation of the methodological contribution, strengths, and limitations of the framework.

5.1. Methodological Contribution and Novelty

The primary contribution of RADAR does not lie in the isolated use of CFD, but in its systematic integration within a conservation-oriented workflow. While previous studies have employed CFD as a case-specific analytical tool, RADAR formalizes a sequential pipeline that connects heritage asset characterization, environmental exposure assessment, analytical scope definition, physics-based simulation, and risk indicator integration into a unified structure. This architecture ensures traceability between climatic drivers, aerodynamic mechanisms, and conservation-relevant risk categories. In particular, the transformation of raw aerodynamic outputs (pressure, wall shear stress, and recirculation patterns) into normalized and spatially integrated degradation proxies represents a methodological advancement. CFD results are not treated as descriptive flow fields but as structured exposure indicators aligned with material vulnerability.

5.2. Strengths of the Framework

A key strength of RADAR is its non-invasive design. In regulatory contexts where direct sampling, intrusive monitoring, or drone-based surveys are restricted, the framework enables exposure-based risk screening using open environmental datasets and physics-based simulation. This approach aligns with conservation principles emphasizing minimum intervention and preservation of authenticity. The framework also demonstrates scalability. Although validated on a large coastal fortification, its modular structure allows adaptation to other CHBS with different typologies and climatic conditions. The explicit coupling of long-term meteorological statistics with representative CFD boundary conditions enhances physical consistency and reduces arbitrariness in scenario selection.

Furthermore, the zone-based assessment stage improves interdisciplinary interpretability. By translating aerodynamic behavior into conservation-relevant categories, the framework facilitates communication between engineers, conservators, and decision-makers.

5.3. Limitations and Assumptions

Despite its advantages, RADAR is subject to certain limitations. The geometric reconstruction adopted in the present study ensures aerodynamic representativeness at the building-envelope scale but does not resolve fine architectural details. Higher-resolution LiDAR or photogrammetric acquisition could refine localized shear stress predictions. Additionally, the steady-state CFD simulation approach captures mean flow behavior but does not represent transient turbulence structures or extreme gust events. While appropriate for long-term exposure assessment, this assumption limits detailed peak-load analysis.

Quantitative validation against long-term material degradation data was not feasible due to regulatory and monitoring constraints. Consequently, the framework currently operates as an exposure-based risk screening tool rather than a predictive deterioration model. Finally, multi-physics processes such as coupled moisture transport, salt crystallization kinetics, and particle impact erosion were not explicitly simulated. Aerodynamic indicators are therefore interpreted as degradation proxies rather than direct material response simulations.

5.4. Implications for Conservation Practice and Future Development

The results confirm that deterioration mechanisms are spatially heterogeneous and strongly governed by orientation, elevation, and geometric discontinuities. This finding supports targeted, mechanism-specific intervention strategies rather than uniform conservation measures. Within the RADAR framework, pressure-dominated zones can inform rain-shielding and drainage optimization, shear-dominated regions may require abrasion-resistant treatments, and recirculation-prone areas demand ventilation-aware preservation planning. Such differentiation enables resource prioritization based on dominant degradation pathways.

Future research should focus on integrating higher-resolution geometric data, incorporating transient wind scenarios, coupling CFD outputs with hygrothermal transport modeling, and embedding RADAR within digital twin environments for continuous monitoring and scenario-based assessment. Overall, RADAR provides a transferable and non-invasive methodology that bridges environmental analysis, numerical simulation, and conservation decision-making, contributing toward more evidence-based management of cultural heritage buildings under environmental stress.

6. Conclusions

This paper introduced RADAR, a non-invasive framework for risk assessment and degradation analysis of cultural heritage buildings that integrates environmental data

analysis, expert-driven material assessment, and computational fluid dynamics modeling. The framework was designed to address a central challenge in heritage conservation: the need to identify deterioration risks and prioritize interventions under strict regulatory and technical constraints that limit invasive monitoring and physical experimentation.

The application of RADAR to the Castle of Mytilene demonstrated how long-term climatic data, air quality indicators, and CFD simulations can be combined to reveal spatially heterogeneous risk patterns. While general environmental stressors such as northerly winds and high relative humidity are known characteristics of the site's geographic setting, the RADAR framework enabled the quantitative identification of how these factors interact with the castle's geometry to produce localized exposure intensification. The results showed that deterioration drivers are not uniformly distributed across the structure but are strongly modulated by orientation, façade configuration, and airflow dynamics resolved through CFD simulation. In particular, wind-driven rain impingement zones, pressure concentration regions, and airflow stagnation areas were identified through the integrated RADAR analysis as key contributors to material degradation, including erosion, salt crystallization, biological growth, and surface weathering.

By coupling measured environmental conditions with physics-based simulations, RADAR moves beyond descriptive environmental assessment and provides a structured, mechanism-oriented interpretation of risk. The zone-level analysis supports targeted mitigation strategies, allowing conservation actions to be prioritized according to dominant degradation pathways rather than applied uniformly across the site. This differentiation is particularly valuable in heritage contexts where financial resources, regulatory permissions, and intervention opportunities are limited.

The methodological results were presented and discussed with professionals involved in heritage documentation and conservation practice related to the monument. The feedback emphasized the practical value of spatial risk differentiation and exposure-based interpretation for supporting preliminary conservation planning. Although the framework has not yet been formally adopted within an official conservation program, it was positively received as a non-intrusive analytical decision-support tool aligned with institutional preservation principles.

Despite its strengths, the proposed framework remains subject to certain limitations. The fidelity of CFD-derived indicators depends on the accuracy of geometric reconstruction, boundary condition definition, and the representativeness of environmental datasets. The steady-state RANS approach captures mean aerodynamic behavior but does not explicitly resolve transient extreme events. Furthermore, long-term quantitative validation against measured material degradation data was not feasible due to regulatory and monitoring constraints. Consequently, RADAR currently functions as an exposure-based risk screening framework rather than a fully predictive deterioration model.

Further methodological development of RADAR is planned to enhance its predictive robustness and operational applicability. Future research will focus on (i) incorporating higher-resolution geometric datasets where permitted, (ii) extending the framework toward multi-scenario and transient wind simulations, (iii) coupling aerodynamic indicators with hygrothermal and salt-transport modeling, (iv) integrating RADAR within digital twin environments to enable continuous environmental risk monitoring and scenario-based conservation assessment.

Overall, RADAR provides a scalable, transferable, and non-intrusive methodology that bridges climatic exposure analysis, numerical simulation, and conservation-oriented interpretation. By translating environmental drivers into spatially differentiated risk categories, the framework contributes toward more resilient, evidence-based, and resource-efficient management of cultural heritage buildings under increasing environmental stress.

Author Contributions: Conceptualization, A.D. and C.-N.A.; methodology, A.D.; software, A.D.; validation, A.D., M.P., O.E. and N.-A.S.; formal analysis, A.D.; investigation, A.D. and N.-A.S.; resources, M.P., R.M. and D.P.-A.; data curation, A.D.; writing—original draft preparation, A.D., O.E. and M.P.; writing—review and editing, A.L., O.E., V.N. and C.-N.A.; visualization, A.D.; supervision, A.L., V.N. and C.-N.A.; project administration, C.-N.A.; funding acquisition, C.-N.A. All authors have read and agreed to the published version of the manuscript.

Funding: This research received no external funding.

Data Availability Statement: Data is included in the text.

Acknowledgments: This research is part of the GATE project funded by the Horizon 2020 WIDESPREAD-2018-2020 TEAMING Phase 2 programme under grant agreement no. 857155 and the programme "Research, Innovation and Digitalization for Smart Transformation" 2021–2027 (PRIDST) under grant agreement no. BG16RFPR002-1.014-0010-C01, and the DS4SSCC–DEP is funded by the European Union Digital Europe Work Programme 2021–2022 under Grant Agreement No. 101123342. The authors gratefully acknowledge the support of the Digital Twin Cities Centre supported by Sweden's Innovation Agency Vinnova [grant number 2024-03904].

Conflicts of Interest: The authors declare no conflicts of interest.

References

1. De Medici, S.; De Toro, P.; Nocca, F. Cultural heritage and sustainable development: Impact assessment of two adaptive reuse projects in Siracusa, Sicily. *Sustainability* **2019**, *12*, 311. [CrossRef]
2. Foster, G.; Saleh, R. The adaptive reuse of cultural heritage in European circular city plans: A systematic review. *Sustainability* **2021**, *13*, 2889. [CrossRef]
3. Naziris, I.A.; Lagaros, N.D.; Papaioannou, K. Optimized fire protection of cultural heritage structures based on the analytic hierarchy process. *J. Build. Eng.* **2016**, *8*, 292–304. [CrossRef]
4. Colace, F.; Gaeta, R.; Lorusso, A.; Pellegrino, M.; Santaniello, D. New AI challenges for cultural heritage protection: A general overview. *J. Cult. Herit.* **2025**, *75*, 168–193. [CrossRef]
5. Liu, R.; Gao, W.; Yang, F. Authenticity, integrity, and cultural–ecological adaptability in heritage conservation: A practical framework for historic urban areas—A case study of Yicheng Ancient City, China. *Buildings* **2025**, *15*, 1304. [CrossRef]
6. Ripp, M.; Clifford, J. Heritage-Based Urban Development. *Encyclopedia* **2025**, *5*, 82. [CrossRef]
7. Aktürk, G.; Hauser, S.J. Integrated understanding of climate change and disaster risk for building resilience of cultural heritage sites. *Nat. Hazards* **2025**, *121*, 4309–4334. [CrossRef]
8. Camuffo, D. *Microclimate for Cultural Heritage*; Elsevier: Amsterdam, The Netherlands, 2019.
9. Thomas, K.; Hardy, R.D.; Lazrus, H.; Mendez, M.; Orlove, B.; Rivera-Collazo, I.; Roberts, J.T.; Rockman, M.; Warner, B.P.; Winthrop, R. Explaining differential vulnerability to climate change: A social science review. *Wiley Interdiscip. Rev. Clim. Chang.* **2019**, *10*, e565. [CrossRef]
10. Adegoriola, M.I.; Lai, J.H.; Chan, E.H.; Darko, A. Heritage building maintenance management (HBMM): A bibliometric-qualitative analysis of literature. *J. Build. Eng.* **2021**, *42*, 102416. [CrossRef]
11. Spyrakos, C.C. Bridging performance based seismic design with restricted interventions on cultural heritage structures. *Eng. Struct.* **2018**, *160*, 34–43. [CrossRef]
12. Phelps, J.R.; Owley, J. Etched in Stone: Historic Preservation Law and Confederate Monuments. *Fla. Law Rev.* **2019**, *71*, 627.
13. Dias Pereira, L.; Tavares, V.; Soares, N. Up-to-date challenges for the conservation, rehabilitation and energy retrofitting of higher education cultural heritage buildings. *Sustainability* **2021**, *13*, 2061. [CrossRef]
14. Luo, L.; Wang, X.; Guo, H.; Lasaponara, R.; Zong, X.; Masini, N.; Wang, G.; Shi, P.; Khatteli, H.; Chen, F.; et al. Airborne and spaceborne remote sensing for archaeological and cultural heritage applications: A review of the century (1907–2017). *Remote Sens. Environ.* **2019**, *232*, 111280. [CrossRef]
15. Napolitano, R.; Riggio, M.; Curmi, A.; Ferreira, T.M.; Pecchioli, L.; Ferrero, C.; Vallis, S.; Chen, X.; Dong, Q.; Giardina, G.; et al. Preserving the Past, Protecting the Future: A Framework for Sustainable Climate Adaptation of Heritage Structures. *Int. J. Archit. Herit.* **2025**, 1–20.. [CrossRef]
16. Yaldiz, E. Climate effects on monumental buildings. In Proceedings of the 4th International Scientific Conference on Water Observation and Information System for Decision Support (BALWOIS), Ohrid, Republic of Macedonia, 25–29 May 2010.
17. Sesana, E.; Gagnon, A.S.; Ciantelli, C.; Cassar, J.; Hughes, J.J. Climate change impacts on cultural heritage: A literature review. *Wiley Interdiscip. Rev. Clim. Chang.* **2021**, *12*, e710. [CrossRef]

18. Kang, H.; Lee, Y.; Kim, S. Sustainable building assessment tool for project decision makers and its development process. *Environ. Impact Assess. Rev.* **2016**, *58*, 34–47. [CrossRef]
19. Hoła, J.; Bień, J.; Schabowicz, K. Non-destructive and semi-destructive diagnostics of concrete structures in assessment of their durability. *Bull. Pol. Acad. Sci. Tech. Sci.* **2015**, *63*, 87–96. [CrossRef]
20. Riggio, M.; Anthony, R.W.; Augelli, F.; Kasal, B.; Lechner, T.; Muller, W.; Tannert, T. In situ assessment of structural timber using non-destructive techniques. *Mater. Struct.* **2014**, *47*, 749–766. [CrossRef]
21. Baduge, S.K.; Thilakarathna, S.; Perera, J.S.; Arashpour, M.; Sharafi, P.; Teodosio, B.; Shringi, A.; Mendis, P. Artificial intelligence and smart vision for building and construction 4.0. *Autom. Constr.* **2022**, *141*, 104440. [CrossRef]
22. Sun, H.; Burton, H.V.; Huang, H. Machine learning applications for building structural design and performance assessment. *J. Build. Eng.* **2021**, *33*, 101816. [CrossRef]
23. Fassi, F.; Fregonese, L.; Ackermann, S.; De Troia, V. Comparison between laser scanning and automated 3D modeling techniques to reconstruct complex and extensive cultural heritage areas. *Int. Arch. Photogramm. Remote Sens. Spat. Inf. Sci.* **2013**, *40*, 73–80. [CrossRef]
24. Yang, J.; You, Y.; Ye, X.; Lin, J. Cultural heritage sites risk assessment based on RS and GIS. *Int. J. Disaster Risk Reduct.* **2023**, *88*, 103593. [CrossRef]
25. Zeng, Z.; Li, L.; Pang, Y. Analysis on climate adaptability of traditional villages in Lingnan, China. *Procedia Eng.* **2017**, *205*, 2011–2018. [CrossRef]
26. Crowley, K.; Jackson, R.; O'connell, S.; Karunarthna, D.; Anantasari, E.; Retnowati, A.; Niem, D. Cultural heritage and risk assessments: Gaps, challenges, and future research directions. *Clim. Resil. Sustain.* **2022**, *1*, e45. [CrossRef]
27. Balci, M.C. Evaluation of deterioration in cultural stone heritage using non-destructive testing techniques: The case of Emir Ali Tomb (Ahlat, Bitlis, Türkiye). *Appl. Sci.* **2025**, *15*, 10404. [CrossRef]
28. Zhang, J.; Wang, G.; Chen, H.; Huang, H.; Shi, Y.; Wang, Q. Internet of things and extended reality in cultural heritage: A review on reconstruction and restoration, intelligent guided tour, and immersive experiences. *IEEE Internet Things J.* **2025**, *12*, 19018–19042. [CrossRef]
29. Xing, Y.; Yang, S.; Fahy, C.; Harwood, T.; Shell, J. Capturing the past, shaping the future: A scoping review of photogrammetry in cultural building heritage. *Electronics* **2025**, *14*, 3666. [CrossRef]
30. Dimabayao, J.J.; Lara, J.L.; Canoura, L.G.; Solheim, S. Integrating climate risk in cultural heritage: A critical review of assessment frameworks. *Heritage* **2025**, *8*, 312. [CrossRef]
31. Guerra-Carrera, L.; Jiménez-Castilla, T.; Segrera-Castilla, M. Cultural heritage, the environment and climate change: Cultural damage from environmental deterioration in San Basilio de Palenque, Colombia. *Soc. Identities* **2025**, *31*, 279–293. [CrossRef]
32. Sanmee, W. Interdisciplinary Approaches to Cultural Conservation: A Model for Sustainable Social Development. *J. Explor. Interdiscip. Methodol. (JEIM)* **2025**, *2*, 1–16.
33. Hussein, A.S.; El-Shishiny, H. Influences of wind flow over heritage sites: A case study of the wind environment over the Giza Plateau in Egypt. *Environ. Model. Softw.* **2009**, *24*, 389–410. [CrossRef]
34. D'Agostino, D.; Congedo, P.M.; Cataldo, R. Computational fluid dynamics (CFD) modeling of microclimate for salts crystallization control and artworks conservation. *J. Cult. Herit.* **2014**, *15*, 448–457. [CrossRef]
35. Wang, X.; Meng, J.; Zhu, T.; Zhang, J. Prediction of Wind Erosion over a Heritage Site: A Case Study of Yongling Mausoleum, China. *Built Herit.* **2019**, *3*, 41–57. [CrossRef]
36. Pineda, P.; Iranzo, A. Analysis of sand-loaded air flow erosion in heritage sites by Computational Fluid Dynamics. *J. Cult. Herit.* **2017**, *25*, 75–86. [CrossRef]
37. Kim, Y. Evaluating environmental factors using microclimate survey and computer fluid dynamics analysis of Korean traditional wooden architectural cultural heritage. *Herit. Sci.* **2023**, *11*, 100. [CrossRef]
38. Dimara, A.; Pantusheva, M.; Mitkov, R.; Naserentin, V.; Spaias, G.; Eleftheriou, O.; Krinidis, S.; Anagnostopoulos, C.-N.; Petrova-Antonova, D.; Logg, A. Non-intrusive Weather Analysis for Sustainable Preservation in Cultural Heritage Buildings. In *IFIP International Conference on Artificial Intelligence Applications and Innovations*; Springer: Cham, Switzerland, 2024; pp. 419–432.
39. Franke, J.; Hellsten, A.; Schlünzen, H.; Carissimo, B. Best Practice Guideline for the CFD Simulation of Flows in the Urban Environment. COST European Cooperation in Science and Technology, Brussels, Belgium, 2007; COST Action 732; p. 52.
40. Tominaga, Y.; Mochida, A.; Yoshie, R.; Kataoka, H.; Nozu, T.; Yoshikawa, M.; Shirasawa, T. AIJ guidelines for practical applications of CFD to pedestrian wind environment around buildings. *J. Wind Eng. Ind. Aerodyn.* **2008**, *96*, 1749–1761. [CrossRef]
41. VDI 3783 Part 9: Environmental Meteorology. Prognostic Microscale Wind Field Models. 2017. Available online: https://www.dinmedia.de/en/technical-rule/vdi-3783-blatt-9/267500591 (accessed on 2 February 2026).
42. Blocken, B. Computational Fluid Dynamics for urban physics. *Build. Environ.* **2015**, *91*, 219–245. [CrossRef]
43. World Map of the Köppen-Geiger Climate Classification Updated. Available online: https://koeppen-geiger.vu-wien.ac.at/pdf/Paper_2006.pdf (accessed on 10 February 2026).

44. Williams, H.; Boyd, T. Investigations at Mytilene and Stymphalos, 1983. *Echos du monde classique: Classical news and views* **1983**, *28*, 169–186.
45. Badouna, I.; Koutsovitis, P.; Laskaridis, K.; Patronis, M.; Papatrechas, C. Aesthetic characteristics of Greek ornamental stones associated with mineral, geochemical and structural properties. *Bull. Geol. Soc. Greece* **2016**, *50*, 1771–1780. [CrossRef]
46. Chen, G.; Dong, Z.; Li, C.; Shi, W.; Shao, T.; Nan, W.; Yang, J. Provenance of aeolian sediments in the Ordos Deserts and its Implication for weathering, sedimentary processes. *Front. Earth Sci.* **2021**, *9*, 711802. [CrossRef]
47. Dueker, M.E.; O'Mullan, G.D.; Martínez, J.M.; Juhl, A.R.; Weathers, K.C. Onshore wind speed modulates microbial aerosols along an urban waterfront. *Atmosphere* **2017**, *8*, 215. [CrossRef]
48. Hatır, M.E. Determining the weathering classification of stone cultural heritage via the analytic hierarchy process and fuzzy inference system. *J. Cult. Herit.* **2020**, *44*, 120–134. [CrossRef]
49. OpenWeather Weather Forecasts, Nowcasts and History in a Fast and Elegant Way. Available online: https://openweathermap.org/history?collection=historical (accessed on 20 January 2024).
50. Dwivedi, R.; Goel, R.; Prasad, V.; Sinha, A. Thermo-mechanical properties of Indian and other granites. *Int. J. Rock Mech. Min. Sci.* **2008**, *45*, 303–315. [CrossRef]
51. Xiang, L.; Meng, Q.; Ren, P. Effects of environmental and architectural factors on chloride-salt deposition on coastal building surfaces in the Zhujiang River Estuary. *Build. Environ.* **2023**, *242*, 110554. [CrossRef]
52. Stefanis, N.A.; Theoulakis, P.; Pilinis, C. Dry deposition effect of marine aerosol to the building stone of the medieval city of Rhodes, Greece. *Build. Environ.* **2009**, *44*, 260–270. [CrossRef]
53. Access to Data | Copernicus—copernicus.eu. Available online: https://www.copernicus.eu/en/access-data (accessed on 27 February 2026).
54. Pantusheva, M.; Mitkov, R.; Hristov, P.O.; Petrova-Antonova, D. Air Pollution Dispersion Modeling in Urban Environment Using CFD: A Systematic Review. *Atmosphere* **2022**, *13*, 1640. [CrossRef]
55. Blocken, B.; Gualtieri, C. Ten iterative steps for model development and evaluation applied to CFD for Environmental Fluid Mechanics. *Environ. Model. Softw.* **2012**, *33*, 1–22. [CrossRef]
56. Richards, P.J.; Hoxey, R.P. Appropriate boundary conditions for computational wind engineering models using the k-epsilon turbulence model. *J. Wind. Eng. Ind. Aerodyn.* **1993**, *46–47*, 145–153. [CrossRef]
57. Richards, P.J.; Norris, S.E. Appropriate boundary conditions for computational wind engineering models revisited. *J. Wind Eng. Ind. Aerodyn.* **2011**, *99*, 257–266. [CrossRef]
58. Richards, P.J.; Norris, S.E. Appropriate boundary conditions for a pressure driven boundary layer. *J. Wind Eng. Ind. Aerodyn.* **2015**, *142*, 43–52. [CrossRef]
59. Richards, P.J.; Norris, S.E. Appropriate boundary conditions for computational wind engineering: Still an issue after 25 years. *J. Wind Eng. Ind. Aerodyn.* **2019**, *190*, 245–255. [CrossRef]
60. Abu-Zidan, Y.; Mendis, P.; Gunawardena, T. Impact of atmospheric boundary layer inhomogeneity in CFD simulations of tall buildings. *Heliyon* **2020**, *6*, e04274. [CrossRef] [PubMed]
61. Parente, A.; Gorlé, C.; van Beeck, J.; Benocci, C. Improved k-epsilon model and wall function formulation for the RANS simulation of ABL flows. *J. Wind Eng. Ind. Aerodyn.* **2011**, *99*, 267–278. [CrossRef]
62. Wieringa, J. Updating the Davenport roughness classification. *J. Wind Eng. Ind. Aerodyn.* **1992**, *41*, 357–368. [CrossRef]
63. Menter, F.R.; Lechner, R.; Matyushenko, A. *Best Practice: Generalized k-ω (GEKO) Two-Equation Turbulence Modeling in Ansys CFD*; ANSYS Inc.: Canonsburg, PA, USA, 2023.
64. Oberkampf, W.L.; Roy, C.J. *Verification and Validation in Scientific Computing*; Cambridge University Press: Cambridge, UK, 2010.

Disclaimer/Publisher's Note: The statements, opinions and data contained in all publications are solely those of the individual author(s) and contributor(s) and not of MDPI and/or the editor(s). MDPI and/or the editor(s) disclaim responsibility for any injury to people or property resulting from any ideas, methods, instructions or products referred to in the content.